THEF-NIJM 98.01
ADP-98-37-T310

Soft-core hyperon-nucleon potentials

Th.A. Rijken
Institute for Theoretical Physics, University of Nijmegen, Nijmegen, The Netherlands

V.G.J. Stoks
Physics Division, Argonne National Laboratory, Argonne, Illinois 60439
and Centre for the Subatomic Structure of Matter, University of Adelaide, SA 5005, Australia

Y. Yamamoto
Physics Section, Tsuru University, Tsuru, Yamanashi 402-0054, Japan
(Published in Phys. Rev. C **59** (1999), 21 – 40)

Abstract

A new Nijmegen soft-core OBE potential model is presented for the low-energy YN interactions. Besides the results for the fit to the scattering data, which largely defines the model, we also present some applications to hypernuclear systems using the G-matrix method. The potentials are generated by the exchange of nonets of pseudoscalar, vector, and scalar mesons. As standard in the Nijmegen soft-core models, we also include the $J = 0$ contributions from the tensor f_2, f_2', a_2 and pomeron Regge trajectories, and use Gaussian form factors to guarantee that the potentials have a soft behavior near the origin. An important innovation with respect to the original soft-core potential is the assignment of the cut-off masses for the baryon-baryon-meson (BBM) vertices in accordance with broken $\mathrm{SU}(3)_F$, which serves to connect the NN and the YN channels. As a novel feature, we allow for medium strong breaking of the coupling constants, using the ${}^3P_0$ model with a Gell-Mann–Okubo hypercharge breaking for the BBM coupling. Charge-symmetry breaking in the Λp and Λn channels is included as well. We present six hyperon-nucleon potentials which describe the available YN cross section data equally well, but which exhibit some differences on a more detailed level. The differences are constructed such that the models encompass a range of scattering lengths in the ΣN and ΛN channels. In all cases, we obtained $\chi^2/N_{\rm data} \approx 0.55$ for 35 YN data. In particular, we were able to fit the precise experimental datum $r_R = 0.468 \pm 0.010$ for the inelastic capture ratio at rest. For the scalar-meson mixing angle we obtained values $\theta_S = 37°$–$40°$, which points to almost ideal mixing angles for the scalar $q\bar{q}$ states. The G-matrix results indicate that the remarkably different spin-spin terms of the six potentials appear specifically in the energy spectra of Λ hypernuclei.

12.39.Pn, 13.75.Ev, 21.30.-x, 21.80.+a

Typeset using REVTEX

I. INTRODUCTION

In Refs. [1,2], henceforth referred to as I and II, respectively, it has been shown that a soft-core one-boson-exchange (OBE) model, based on Regge-pole theory [3], provides an excellent simultaneous description of the rich and accurate nucleon-nucleon (NN) and the more scarce hyperon-nucleon (YN) low-energy scattering data. However, in the application to the hypernuclear systems using the G-matrix method, it was found that the spin-spin interaction in the ΛN channels needs a correction [4–6]. Another inconvenience with I and II is that an extension to the $\Lambda\Lambda$ and ΞN channels cannot be done without the introduction of extra free parameters.

In order to improve the soft-core interaction on these points, we here modify the original soft-core OBE models of I and II in the following way. First, we assign the cut-off parameters in the form factors for the individual baryon-baryon-meson (BBM) vertices, constrained by broken $\mathrm{SU}(3)_F$ symmetry. This in contrast to I and II, where these cut-off parameters were assigned per baryon-baryon $\mathrm{SU}(3)_F$-irrep. Because the $\Lambda\Lambda$ and ΞN channels involve the $\{1\}$-irrep, which does not occur in the NN and YN channels, the description of these channels would require the introduction of additional free parameters. However, there are no experimental scattering data to determine these parameters. (The only experimental information on the $\Lambda\Lambda$ interaction is limited to the ground states of double-Λ hypernuclei, but such information is "contaminated" by few-body effects.) Second, we note that in Ref. [2] the magnetic $F/(F+D)$ ratio α_V^m for the vector mesons was fixed to its SU(6) value. Therefore, in order to improve the spin-spin interaction, we here consider α_V^m as a free input and make fits for different values of this parameter. It turns out that this allows us to construct YN models which encompass a range of scattering lengths in the $^1S_0$ and the $^3S_1$ ΛN channels. It is found that various other quantities, calculated with these new models, also exhibit an impressive correlation with the choice for α_V^m. By testing these models in hypernuclear systems we can select the successful spin-spin interaction. In order to have enough flexibility, we introduced a third modification with respect to I and II; namely, we allow for medium strong breaking of the coupling constants. The breaking is implemented according to the $^3P_0$ model [7] with a Gell-Mann–Okubo hypercharge breaking.

Apart from the modifications indicated above, the OBE models of this paper, henceforth referred to as NSC97 models, are motivated according to the same physical principles as those of I and II. We refer to the latter papers [1,2] for a more detailed description of the physics background of the Nijmegen soft-core baryon-baryon models. We here only briefly reiterate the main points.

The baryon-baryon soft-core models can be fully derived in the context of the analytical S-matrix theory [3]. This seems a proper framework to describe baryons and mesons, which are composite particles. In particular, in QCD the mesons are $q\bar{q}$ systems and any reasonable interaction used in a Bethe-Salpeter approach to the $q\bar{q}$ systems leads to mesons on Regge trajectories. The consequences of the Regge trajectories for low-energy scattering and the corresponding (relativistic) Lippmann-Schwinger equations can be worked out in a consistent manner in the mentioned framework.

With a combined treatment of the NN and YN channels we aim at a high-quality description of the baryon-baryon interactions. By high quality we mean a fit to the YN scattering data with a low χ^2, such that, while keeping the constraints forced on the potentials by the fit to the NN scattering data, the free parameters with a clear physical significance (like, e.g., the $F/(F+D)$ ratios α_{PV} and α_V^m) assume realistic values. Such a combined study of all baryon-baryon interactions, and especially NN and YN, is desirable if one wants to test the assumption of $\mathrm{SU}(3)_F$ symmetry. For example, we want to investigate the properties of the scalar mesons [$\varepsilon(760)$, $f_0(975)$, $a_0(980)$, $\kappa(880)$], since especially the status of the scalar nonet is at present not established yet. We also want to extract information about scattering lengths, effective ranges, and the existence of resonances. This, in spite of the scarce experimental YN data. Moreover, we aim to extend the theoretical description to the $\Lambda\Lambda$ and ΞN channels, where experiments may be realized in the foreseeable future.

In this paper we treat in detail the following YN reactions for which experimental data exist: (i) The coupled-channel reaction $\Lambda p \Rightarrow \Lambda p, \Sigma^+ n, \Sigma^0 p$, below the threshold of the coupling to the ΣN channels; (ii) The coupled-channel reaction $\Sigma^- p \Rightarrow \Lambda n, \Sigma^0 n, \Sigma^- p$, and (iii) The single-channel reaction $\Sigma^+ p \Rightarrow \Sigma^+ p$. The NSC97 models of this paper are a step forward in the realization of a program where the baryon-baryon interactions for scattering and hypernuclei can be described in the context of broken $\mathrm{SU}(3)_F$ symmetry.

For definiteness, we list the meson exchanges which are included:

(i) The pseudoscalar mesons (π, η, η', K), with the η–η' mixing angle $\theta_{PV} = -23.0^0$ from the Gell-Mann–Okubo mass formula. The $F/(F+D)$ ratio, $\alpha_{PV} = 0.355$, is given by the value found in semileptonic weak decays [8].

(ii) The vector mesons (ρ, ϕ, ω, $K^\star$), with the ϕ–ω mixing angle $\theta_V = 37.5°$ [8] and the electric $\alpha_V^e = 1$, which follows the "universality" assumption [9]. The magnetic α_V^m is used as a free input to encompass a range of scattering lengths, characterizing the different models, but is restricted to values consistent with static or relativistic SU(6) predictions [10].

(iii) The scalar mesons [$a_0(980)$, $f_0(975)$, $f_0(760)$, $\kappa(880)$]. In the following, we will reserve f_0 for the $f_0(975)$ meson and use ε for the $f_0(760)$ meson. The free f_0–ε mixing angle θ_S is to be determined in the fit to the YN data.

(iv) The "diffractive" contribution from the pomeron P and from the tensor mesons [$f_2(1285)$, $f_2'(1525)$, $a_2(1270)$]. These exchanges will give repulsive contributions of a Gaussian type.

The BBM vertices are described by coupling constants and form factors, which correspond to the Regge residues at high energies [3]. The form factors are taken to be of the Gaussian type, like the residue functions in many Regge-pole models for high-energy scattering. Note that also in (nonrelativistic) quark models a Gaussian behavior of the form factors is most natural. These form factors evidently guarantee a soft behavior of the potentials in configuration space at small distances.

It turns out that, starting from the soft-core OBE model for the NN interaction, we are indeed able to achieve a very good description of the YN data, and at the same time maintain values for the free parameters which are consistent with the present view on low-energy hadron physics. Like in I and II we use $\mathrm{SU}(3)_F$ symmetry for the coupling constants, while $\mathrm{SU}(3)_F$ breaking is included by (i) using the physical masses of the mesons and baryons in the potentials and in the Schrödinger equation; (ii) allowing for meson-mixing within a nonet (η–η', ω–ϕ, ε–f_0); (iii) including charge-symmetry breaking (CSB) due to Λ-Σ^0 mixing [11], which introduces a one-pion-exchange (OPE) potential in the Λp and Λn channels; and (iv) taking into account the Coulomb interaction. In order to include the Coulomb interaction exactly, and to account as much as possible for the mass differences between the baryons, we solve the multichannel Schrödinger equation on the physical particle basis. However, in order to limit the number of different form factors, the nuclear potentials are calculated on the isospin basis. This means that we include only the so-called "medium strong" $\mathrm{SU}(3)_F$ breaking in the potentials.

The content of this paper is as follows. In Sec. II we give the meson-baryon interaction Lagrangian and define the OBE potentials for the Lippmann-Schwinger equation. In Sec. III we review the possible YN channels that are allowed and discuss some aspects of the multichannel Schrödinger equation. In Sec. IV we discuss the pseudoscalar- and vector-meson multiplets. The scalar-meson multiplet is discussed rather extensively, because of its important role in the soft-core OBE models. Also, some remarks are made on the origin and nature of the pomeron and tensor-meson contributions. In Sec. V we outline the broken $\mathrm{SU}(3)_F$ scheme of the form factors and the coupling constants, in particular the employed $^3P_0$ model. Section VI contains the results of the fits to the YN scattering data, while in Sec. VII the properties of the models are investigated in hypernuclear systems within the G-matrix approach. Finally, in Sec. VIII we finish with a final discussion and draw some conclusions.

II. DEFINITION OF THE POTENTIALS

The nucleon-nucleon (NN) and hyperon-nucleon (YN) potentials constitute only a subset of possible interaction channels for the baryon-baryon interaction; they cover only the strangeness $S = 0, -1$ channels. The various members of the baryon octet, in principle, allow for baryon-baryon interactions with total strangeness up to $S = -4$. Since at present there are no scattering data for the $S = -2$, -3, and -4 channels, any results based on these potentials are pure predictions and hence will be left for a future publication. Here we only focus on the $S = -1$ channel, for which scattering data do exist. However, because our models heavily rely on the assumption of SU(3) symmetry (although we allow for a breaking of this symmetry to allow for the fact that the strange quark is much heavier than the up and down quarks), we will here define the interaction Lagrangian, and hence the coupling constants, for the complete baryon octet.

The eight $J^P = \frac{1}{2}^+$ baryons can be collected into a traceless matrix B, which has the familiar form

$$B = \begin{pmatrix} \dfrac{\Sigma^0}{\sqrt{2}} + \dfrac{\Lambda}{\sqrt{6}} & \Sigma^+ & p \\ \Sigma^- & -\dfrac{\Sigma^0}{\sqrt{2}} + \dfrac{\Lambda}{\sqrt{6}} & n \\ -\Xi^- & \Xi^0 & -\dfrac{2\Lambda}{\sqrt{6}} \end{pmatrix}, \tag{2.1}$$

and which is invariant under SU(3) transformations. Similarly, the various meson nonets (we take the pseudoscalar mesons with $J^P = 0^+$ as an example) can be written as

$$P = P_{\rm sin} + P_{\rm oct}, \tag{2.2}$$

where the singlet matrix $P_{\rm sin}$ has elements $\eta_0/\sqrt{3}$ on the diagonal, and the octet matrix $P_{\rm oct}$ is given by

$$
P_{\rm oct} = \begin{pmatrix} \dfrac{\pi^0}{\sqrt{2}} + \dfrac{\eta_8}{\sqrt{6}} & \pi^+ & K^+ \\ \pi^- & -\dfrac{\pi^0}{\sqrt{2}} + \dfrac{\eta_8}{\sqrt{6}} & K^0 \\ K^- & \overline{K^0} & -\dfrac{2\eta_8}{\sqrt{6}} \end{pmatrix} . \tag{2.3}
$$

One can now define the SU(3)-invariant combinations

$$
\begin{aligned}
\left[\overline{B}BP\right]_F &= {\rm Tr}(\overline{B}PB) - {\rm Tr}(\overline{B}BP) \\
&= {\rm Tr}(\overline{B}P_{\rm oct}B) - {\rm Tr}(\overline{B}BP_{\rm oct}), && (2.4) \\
\left[\overline{B}BP\right]_D &= {\rm Tr}(\overline{B}PB) + {\rm Tr}(\overline{B}BP) - \tfrac{2}{3}\,{\rm Tr}(\overline{B}B){\rm Tr}(P) \\
&= {\rm Tr}(\overline{B}P_{\rm oct}B) + {\rm Tr}(\overline{B}BP_{\rm oct}), && (2.5) \\
\left[\overline{B}BP\right]_S &= {\rm Tr}(\overline{B}B){\rm Tr}(P) \\
&= {\rm Tr}(\overline{B}B){\rm Tr}(P_{\rm sin}), && (2.6)
\end{aligned}
$$

and hence an interaction Lagrangian [12]

$$
\mathcal{L}_I = -g^{\rm oct}\sqrt{2}\left\{\alpha\left[\overline{B}BP\right]_F + (1-\alpha)\left[\overline{B}BP\right]_D\right\} - g^{\rm sin}\sqrt{\tfrac{1}{3}}\left[\overline{B}BP\right]_S , \tag{2.7}
$$

where α is known as the $F/(F+D)$ ratio, and the square-root factors are introduced for later convenience. We next introduce the isospin doublets

$$
N = \begin{pmatrix} p \\ n \end{pmatrix}, \quad \Xi = \begin{pmatrix} \Xi^0 \\ \Xi^- \end{pmatrix}, \quad K = \begin{pmatrix} K^+ \\ K^0 \end{pmatrix}, \quad K_c = \begin{pmatrix} \overline{K^0} \\ -K^- \end{pmatrix}, \tag{2.8}
$$

and choose the phases of the isovector meson fields $\boldsymbol{\Sigma}$ and $\boldsymbol{\pi}$ such [12] that

$$
\boldsymbol{\Sigma}\cdot\boldsymbol{\pi} = \Sigma^+\pi^- + \Sigma^0\pi^0 + \Sigma^-\pi^+ . \tag{2.9}
$$

If we now drop for a moment the Lorentz character of the interaction vertices ($\gamma_5\gamma_\mu\partial^\mu$ for pseudoscalar mesons), the pseudovector-coupled (derivative) pseudoscalar-meson interaction Lagrangian is of the form

$$
\mathcal{L}_{\rm pv} = \mathcal{L}_{\rm pv}^{\rm sin} + \mathcal{L}_{\rm pv}^{\rm oct} , \tag{2.10}
$$

where the S-type coupling in Eq. (2.7) gives the singlet interaction Lagrangian

$$
m_\pi \mathcal{L}_{\rm pv}^{\rm sin} = -f_{NN\eta_0}(\overline{N}N)\eta_0 - f_{\Lambda\Lambda\eta_0}(\overline{\Lambda}\Lambda)\eta_0 - f_{\Sigma\Sigma\eta_0}(\overline{\boldsymbol{\Sigma}}\cdot\boldsymbol{\Sigma})\eta_0 - f_{\Xi\Xi\eta_0}(\overline{\Xi}\Xi)\eta_0 , \tag{2.11}
$$

with the (derivative) pseudovector coupling constants

$$
f_{NN\eta_0} = f_{\Lambda\Lambda\eta_0} = f_{\Sigma\Sigma\eta_0} = f_{\Xi\Xi\eta_0} = f_{\rm pv}^{\rm sin} . \tag{2.12}
$$

As is customary [8], we introduced the charged-pion mass as a scaling mass to make the pseudovector coupling constants f dimensionless. The interaction Lagrangian for the meson octet is obtained by evaluating the F- and D-type couplings in Eq. (2.7), and can be written as

$$\begin{aligned} m_\pi \mathcal{L}_{\rm pv}^{\rm oct} = & -f_{NN\pi}(\overline{N}\boldsymbol{\tau}N)\cdot\boldsymbol{\pi} + i f_{\Sigma\Sigma\pi}(\overline{\boldsymbol{\Sigma}}\times\boldsymbol{\Sigma})\cdot\boldsymbol{\pi} - f_{\Lambda\Sigma\pi}(\overline{\Lambda}\boldsymbol{\Sigma}+\overline{\boldsymbol{\Sigma}}\Lambda)\cdot\boldsymbol{\pi} - f_{\Xi\Xi\pi}(\overline{\Xi}\boldsymbol{\tau}\Xi)\cdot\boldsymbol{\pi} \\ & -f_{\Lambda NK}\left[(\overline{N}K)\Lambda + \overline{\Lambda}(\overline{K}N)\right] - f_{\Xi\Lambda K}\left[(\overline{\Xi}K_c)\Lambda + \overline{\Lambda}(\overline{K_c}\Xi)\right] \\ & -f_{\Sigma NK}\left[\overline{\boldsymbol{\Sigma}}\cdot(\overline{K}\boldsymbol{\tau}N) + (\overline{N}\boldsymbol{\tau}K)\cdot\boldsymbol{\Sigma}\right] - f_{\Xi\Sigma K}\left[\overline{\boldsymbol{\Sigma}}\cdot(\overline{K_c}\boldsymbol{\tau}\Xi) + (\overline{\Xi}\boldsymbol{\tau}K_c)\cdot\boldsymbol{\Sigma}\right] \\ & -f_{NN\eta_8}(\overline{N}N)\eta_8 - f_{\Lambda\Lambda\eta_8}(\overline{\Lambda}\Lambda)\eta_8 - f_{\Sigma\Sigma\eta_8}(\overline{\boldsymbol{\Sigma}}\cdot\boldsymbol{\Sigma})\eta_8 - f_{\Xi\Xi\eta_8}(\overline{\Xi}\Xi)\eta_8. \end{aligned} \tag{2.13}$$

The octet coupling constants are given by the following expressions ($f \equiv f_{\rm pv}^{\rm oct}$)

$$\begin{array}{lll} f_{NN\pi} = f, & f_{\Lambda NK} = -\frac{1}{\sqrt{3}}\,f(1+2\alpha), & f_{NN\eta_8} = \frac{1}{\sqrt{3}}\,f(4\alpha-1), \\ f_{\Sigma\Sigma\pi} = 2f\alpha, & f_{\Xi\Lambda K} = \frac{1}{\sqrt{3}}\,f(4\alpha-1), & f_{\Lambda\Lambda\eta_8} = -\frac{2}{\sqrt{3}}\,f(1-\alpha), \\ f_{\Lambda\Sigma\pi} = \frac{2}{\sqrt{3}}\,f(1-\alpha), & f_{\Sigma NK} = f(1-2\alpha), & f_{\Sigma\Sigma\eta_8} = \frac{2}{\sqrt{3}}\,f(1-\alpha), \\ f_{\Xi\Xi\pi} = -f(1-2\alpha), & f_{\Xi\Sigma K} = -f, & f_{\Xi\Xi\eta_8} = -\frac{1}{\sqrt{3}}\,f(1+2\alpha). \end{array} \tag{2.14}$$

Similar relations (without the scaling mass m_π) are found for the coupling constants of the scalar and vector mesons.

The assumption of SU(3) symmetry thus implies that for each type of meson (pseudoscalar, vector, scalar) we need only four parameters to characterize their couplings with all possible baryons: the singlet coupling constant, the octet coupling constant, the $F/(F+D)$ ratio, and a mixing angle which relates the physical isoscalar mesons to their pure octet and singlet counterparts. However, it is not *a priori* obvious that these SU(3) relations for the coupling constants will be satisfied exactly. For example, the strange quark is much heavier than the up and down quarks, and so already on the quark-mass level the SU(3) symmetry is clearly broken.

In our models, breaking of the SU(3) symmetry is introduced in several places as well. First of all, we use the physical masses for the baryons and mesons. Second, we allow for the fact that the Λ and Σ^0 have the same quark content, and so there is an appreciable mixing between the isospin-pure Λ and Σ^0 states [11]. Although exact SU(3) symmetry requires that $f_{\Lambda\Lambda\pi^0} = 0$, Λ-Σ^0 mixing and the interaction $\Sigma^0 \to \Lambda + \pi^0$ result in a non-zero pion coupling constant for the physical Λ-hyperon. Dalitz and von Hippel derive [11]

$$f_{\Lambda\Lambda\pi} = -2\frac{\langle\Sigma^0|\delta M|\Lambda\rangle}{M_{\Sigma^0}-M_\Lambda}\,f_{\Lambda\Sigma\pi}, \tag{2.15}$$

where the $\Sigma\Lambda$ element of the electromagnetic mass matrix is given by

$$\langle\Sigma^0|\delta M|\Lambda\rangle = \left[M_{\Sigma^0} - M_\Lambda + M_p - M_n\right]/\sqrt{3}. \tag{2.16}$$

Substituting for the physical baryon masses, we find

$$f_{\Lambda\Lambda\pi} = -0.0283\,f_{\Lambda\Sigma\pi}. \tag{2.17}$$

Writing out the nucleon-nucleon-pion part of the interaction Lagrangian (2.13), we find

$$(\overline{N}\boldsymbol{\tau}N)\cdot\boldsymbol{\pi} = \overline{p}p\pi^0 - \overline{n}n\pi^0 + \sqrt{2}\,\overline{p}n\pi^+ + \sqrt{2}\,\overline{n}p\pi^-, \tag{2.18}$$

and so the neutral pion is seen to couple to the neutron with opposite sign as compared to its coupling to the proton. This implies that the non-zero $f_{\Lambda\Lambda\pi^0}$ coupling produces strong deviations from charge symmetry for the Λp and Λn potentials. Obviously, Λ-Σ^0 mixing also gives non-zero $\Lambda\Lambda$ coupling constants for the other neutral isovector mesons, but they give rise to much smaller effects.

Finally, we use the $^3P_0$ model [7,13] to account for the fact that the strange quark is much heavier than the up and down quarks. In this model, the breaking of the SU(3)-flavor symmetry is described by one parameter $\lambda_{\rm fsb}$, where we allow for a different parameter for each meson nonet. This will be discussed in more detail in Sec. V.

In order to define the potential in momentum space, we next consider the general baryon-baryon scattering reaction

$$B_1(p_1) + B_2(p_2) \rightarrow B_3(p_3) + B_4(p_4), \tag{2.19}$$

where the four-momentum of baryon B_i is $p_i = (E_i, \mathbf{p}_i)$, with $E_i = \sqrt{\mathbf{p}_i^2 + M_i^2}$ and M_i its mass. The second-order one-meson-exchange kernel is derived following the procedure as discussed in our earlier papers on two-meson exchange [14,15], to which we refer for details and definitions. In this procedure the Thompson equation [16] for the wave function reads

$$\phi_{++}(\mathbf{p}') = \phi_{++}^{(0)}(\mathbf{p}') + E_2^{(+)}(\mathbf{p}';W)\int d^3p K^{\rm irr}(\mathbf{p}',\mathbf{p}|W)\phi_{++}(\mathbf{p}), \tag{2.20}$$

with $W=\sqrt{s}$ the total energy, and $\mathbf{p}$ and $\mathbf{p}'$ the center-of-mass momenta in the initial and final states, respectively. The irreducible kernel is given by

$$\begin{aligned} K^{\rm irr}(\mathbf{p}',\mathbf{p}|W) = &-(2\pi)^2\,[W-E_3(\mathbf{p}')-E_4(\mathbf{p}')]\;[W-E_1(\mathbf{p})-E_2(\mathbf{p})]\int_{-\infty}^{\infty}dp_0'\int_{-\infty}^{\infty}dp_0 \\ &\times\left\{\left[F_W^{(3)}(\mathbf{p}',p_0')F_W^{(4)}(-\mathbf{p}',-p_0')\right]^{-1}[I(\mathbf{p}',p_0';\mathbf{p},p_0)]_{++,++}\left[F_W^{(1)}(\mathbf{p},p_0)F_W^{(2)}(-\mathbf{p},-p_0)\right]^{-1}\right\}. \end{aligned} \tag{2.21}$$

Substituting for the one-meson-exchange Feynman propagator and performing the p_0 and p_0' integrations generates the two time-ordered one-meson-exchange diagrams with energy denominator

$$D(\omega) = \frac{1}{2\omega}\left[\frac{1}{E_2+E_3-W+\omega} + \frac{1}{E_1+E_4-W+\omega}\right]. \tag{2.22}$$

Here, $\omega^2 = \mathbf{k}^2 + m^2$, with m the meson mass and $\mathbf{k} = \mathbf{p}'-\mathbf{p}$ the momentum transfer. In the static approximation $E_i \rightarrow M_i$ and $W \rightarrow M_1^0 + M_2^0$. Note that we have included a superscript 0 to indicate that these masses refer to the masses of the particular interaction channel we are considering. They are not necessarily equal to the masses M_1 and M_2 occurring in the time-ordered diagrams. For example, the potential for the $\Sigma N \rightarrow \Sigma N$ contribution in the coupled-channel $(\Lambda N, \Sigma N)$ system has $M_1 = M_\Sigma$ and $M_2 = M_N$, but $M_1^0 = M_\Lambda$ and $M_2^0 = M_N$.

In principle, the propagator in the static approximation can be handled exactly using the fact that [14]

$$\frac{1}{\omega(\omega+a)} = \frac{2}{\pi}\int_0^\infty \frac{a\,d\lambda}{(\omega^2+\lambda^2)(a^2+\lambda^2)} + \frac{2\theta(-a)}{\omega^2-a^2}, \quad (a<m). \tag{2.23}$$

However, this requires an additional (numerical) evaluation of an integral whenever $a \neq 0$, which might be a considerable time factor in practical calculations. A way to avoid this additional integral is to assume that the average of the initial and final masses always approximately equals the mass of the interaction channel, $M_1^0 + M_2^0$. The advantage of this, more crude, approximation is that the propagator can then be written as

$$D(\omega) \to \frac{1}{\omega^2 - \frac{1}{4}(M_3 - M_4 + M_2 - M_1)^2}, \tag{2.24}$$

which means we have introduced an effective meson mass $\overline{m}$, where the mass has dropped to

$$m^2 \to \overline{m}^2 = m^2 - \tfrac{1}{4}(M_3 - M_4 + M_2 - M_1)^2. \tag{2.25}$$

The change in mass can be considerable for certain potentials. For example, the effective kaon mass in $\Sigma N \to N\Sigma$ drops from 495.8 MeV/c^2 to 425.8 MeV/c^2. In the following, we will use the static approximation in the form of Eq. (2.24). In view of the relatively large error bars on the experimental YN scattering data, we argue that at present it is not worthwhile to pursue the more complicated exact treatment; we leave this for a later study. Note also that this approximation still ensures that the potential, viewed as a matrix in channel space, is symmetric, as required by time-reversal invariance.

The transition from the Thompson equation (2.20) to the Lippmann-Schwinger equation,

$$\phi(\mathbf{p}') = \phi^{(0)}(\mathbf{p}') + g(\mathbf{p}';W)\int d^3p V(\mathbf{p}',\mathbf{p}|W)\phi(\mathbf{p}), \tag{2.26}$$

is made by defining the transformations

$$\phi_{++}(\mathbf{p}) = N(\mathbf{p};W)\phi(\mathbf{p}),$$

$$K^{\mathrm{irr}}(\mathbf{p}',\mathbf{p}|W) = N^{-1}(\mathbf{p}';W)V(\mathbf{p}',\mathbf{p}|W)N^{-1}(\mathbf{p};W),$$

$$E_2^{(+)}(\mathbf{p};W) = N^2(\mathbf{p};W)g(\mathbf{p};W), \tag{2.27}$$

with the Green's function

$$g(\mathbf{p};W) = \frac{1}{(2\pi)^3}\Lambda_+^{(1)}(\mathbf{p})\Lambda_+^{(2)}(\mathbf{p})\frac{2M_{\mathrm{red}}}{\mathbf{p}_i^2 - \mathbf{p}^2 + i\delta}, \tag{2.28}$$

with $\Lambda_+(\mathbf{p})$ a spin-projection operator and $\mathbf{p}_i$ the on-shell momentum associated with W. This defines the potential. We make the standard expansions and approximations valid for low-energy scattering and end up with the potentials as given in Ref. [2][1]. The partial-wave projection for the momentum-space potential is discussed in Ref. [17].

The potentials are regularized with a Gaussian cut off, which still allows for the Fourier transform to configuration space to be carried out analytically. Details again can be found in Ref. [2]. Unfortunately, this reference contains a number of typographical errors. The corrected expressions are given in the appendix, where the potentials refer to the scattering process where one of the meson vertices occurs between B_1 and B_3, and the other between B_2 and B_4. The mass M_{13} then denotes the average of the B_1 and B_3 masses, and M_{24} the average of the B_2 and B_4 masses. For the exchanged diagram we have to interchange $3 \leftrightarrow 4$ everywhere and multiply by the exchange operator P. The exchange operator $P = +1$ for even-L singlet and odd-L triplet partial waves, and $P = -1$ for odd-L singlet and even-L triplet partial waves. For YN scattering, the exchanged diagram only occurs when the exchanged meson carries strangeness (K, K^*, κ, K^{**}).

III. *YN* CHANNELS

In our approach, the potentials are calculated on the isospin basis. Because the two nucleons form an isodoublet, the Λ-hyperon an isosinglet, and the three Σ-hyperons an isotriplet, there are only two isospin channels:

$$\begin{aligned} I = \tfrac{1}{2}: &\quad (\Lambda N, \Sigma N) \to (\Lambda N, \Sigma N), \\ I = \tfrac{3}{2}: &\quad \Sigma N \to \Sigma N. \end{aligned} \tag{3.1}$$

The isospin factors for the various meson exchanges in the two isospin channels are given in Table I. We use the pseudoscalar mesons as a specific example, and P is the exchange operator alluded to in the previous section. We also include the coupling of the Λ-hyperon to the neutral pion, which is non-zero due to Λ-Σ^0 mixing, as was discussed earlier. However, this matrix element is *only* included when the potentials are used for calculations on the physical particle basis.

In the physical particle basis, there are four charge channels:

$$\begin{aligned} q = +2: &\quad \Sigma^+ p \to \Sigma^+ p, \\ q = +1: &\quad (\Lambda p, \Sigma^+ n, \Sigma^0 p) \to (\Lambda p, \Sigma^+ n, \Sigma^0 p), \\ q = \;\;\, 0: &\quad (\Lambda n, \Sigma^0 n, \Sigma^- p) \to (\Lambda n, \Sigma^0 n, \Sigma^- p), \\ q = -1: &\quad \Sigma^- n \to \Sigma^- n. \end{aligned} \tag{3.2}$$

Obviously, the potential on the particle basis for the $q = 2$ and $q = -1$ channels are given by the $I = \frac{3}{2}$ ΣN potential on the isospin basis, substituting the appropriate physical particle masses. For $q = 1$ and $q = 0$, the potentials are related to the potentials on the

[1] Note that in Ref. [2], $\Omega_2^{(P)}$ in Eq. (23) should have a minus sign and $\Omega_6^{(S)}$ in Eq. (25) should have masses squared in the denominator.

isospin basis by an isospin rotation. Using a notation where we only list the hyperons $[V_{\Lambda\Sigma^+} = (\Lambda p|V|\Sigma^+ n)$, etc.], we find for $q = 1$

$$\begin{pmatrix} V_{\Lambda\Lambda} & V_{\Lambda\Sigma^+} & V_{\Lambda\Sigma^0} \\ V_{\Sigma^+\Lambda} & V_{\Sigma^+\Sigma^+} & V_{\Sigma^+\Sigma^0} \\ V_{\Sigma^0\Lambda} & V_{\Sigma^0\Sigma^+} & V_{\Sigma^0\Sigma^0} \end{pmatrix} = \begin{pmatrix} V_{\Lambda\Lambda} & \sqrt{\frac{2}{3}}V_{\Lambda\Sigma} & -\sqrt{\frac{1}{3}}V_{\Lambda\Sigma} \\ \sqrt{\frac{2}{3}}V_{\Sigma\Lambda} & \frac{2}{3}V_{\Sigma\Sigma}(\frac{1}{2}) + \frac{1}{3}V_{\Sigma\Sigma}(\frac{3}{2}) & \frac{1}{3}\sqrt{2}\left[V_{\Sigma\Sigma}(\frac{3}{2}) - V_{\Sigma\Sigma}(\frac{1}{2})\right] \\ -\sqrt{\frac{1}{3}}V_{\Sigma\Lambda} & \frac{1}{3}\sqrt{2}\left[V_{\Sigma\Sigma}(\frac{3}{2}) - V_{\Sigma\Sigma}(\frac{1}{2})\right] & \frac{1}{3}V_{\Sigma\Sigma}(\frac{1}{2}) + \frac{2}{3}V_{\Sigma\Sigma}(\frac{3}{2}) \end{pmatrix}, \tag{3.3}$$

while for $q = 0$ we find

$$\begin{pmatrix} V_{\Lambda\Lambda} & V_{\Lambda\Sigma^0} & V_{\Lambda\Sigma^-} \\ V_{\Sigma^0\Lambda} & V_{\Sigma^0\Sigma^0} & V_{\Sigma^0\Sigma^-} \\ V_{\Sigma^-\Lambda} & V_{\Sigma^-\Sigma^0} & V_{\Sigma^-\Sigma^-} \end{pmatrix} = \begin{pmatrix} V_{\Lambda\Lambda} & \sqrt{\frac{1}{3}}V_{\Lambda\Sigma} & -\sqrt{\frac{2}{3}}V_{\Lambda\Sigma} \\ \sqrt{\frac{1}{3}}V_{\Sigma\Lambda} & \frac{1}{3}V_{\Sigma\Sigma}(\frac{1}{2}) + \frac{2}{3}V_{\Sigma\Sigma}(\frac{3}{2}) & \frac{1}{3}\sqrt{2}\left[V_{\Sigma\Sigma}(\frac{3}{2}) - V_{\Sigma\Sigma}(\frac{1}{2})\right] \\ -\sqrt{\frac{2}{3}}V_{\Sigma\Lambda} & \frac{1}{3}\sqrt{2}\left[V_{\Sigma\Sigma}(\frac{3}{2}) - V_{\Sigma\Sigma}(\frac{1}{2})\right] & \frac{2}{3}V_{\Sigma\Sigma}(\frac{1}{2}) + \frac{1}{3}V_{\Sigma\Sigma}(\frac{3}{2}) \end{pmatrix}. \tag{3.4}$$

The relativistic relation between the on-shell center-of-mass momentum p_i in channel i and the total energy $\sqrt{s}$ is given by

$$p_i^2 = \frac{1}{4s}\left[s - (M_1(i) + M_2(i))^2\right]\left[s - (M_1(i) - M_2(i))^2\right], \tag{3.5}$$

while the total energy squared for a specific interaction channel i with laboratory momentum $p_{\rm lab}(i)$ is given by

$$s = M_1^2(i) + M_2^2(i) + 2M_2(i)\sqrt{p_{\rm lab}^2(i) + M_1^2(i)}. \tag{3.6}$$

Expanding the square-root energies, we obtain the corresponding nonrelativistic expressions:

$$\begin{aligned} p_i^2 &= 2M_{\rm red}(i)\left[\sqrt{s} - M_1(i) - M_2(i)\right], \\ \sqrt{s} &= M_1(i) + M_2(i) + M_{\rm red}(i)\left[p_{\rm lab}^2(i)/2M_1^2(i)\right]. \end{aligned}$$

We always use the relativistic relations (3.5) and (3.6). Substituting for the empirical baryon masses, the various ΣN thresholds in the Λp channel are found to be at

$$p_{\rm lab}^{\rm th}(\Lambda p \to \Sigma^+ n) = 633.4 \text{ MeV}/c, \quad p_{\rm lab}^{\rm th}(\Lambda p \to \Sigma^0 p) = 642.0 \text{ MeV}/c; \tag{3.7}$$

those in the Λn channel at

$$p_{\rm lab}^{\rm th}(\Lambda n \to \Sigma^0 n) = 641.7 \text{ MeV}/c, \quad p_{\rm lab}^{\rm th}(\Lambda n \to \Sigma^- p) = 657.9 \text{ MeV}/c; \tag{3.8}$$

and the average (single) threshold for the potential on the isospin basis at

$$p_{\rm lab}^{\rm th}(\Lambda N \to \Sigma N) = 643.8 \text{ MeV}/c. \tag{3.9}$$

Using nonrelativistic kinematics, the thresholds are found to be lower by about 30 MeV/c.

There are various ways to solve the Lippmann-Schwinger equation for the partial-wave momentum-space potential. We use the Kowalski-Noyes method [18,19] to handle the singularities in the Green's function for the open channels. The Coulomb interaction in the $\Sigma^+ p \rightarrow \Sigma^+ p$ and $\Sigma^- p \rightarrow \Sigma^- p$ channels is included via the Vincent-Phatak method [20].

The multichannel Schrödinger equation for the configuration-space potential is derived from the Lippmann-Schwinger equation through the standard Fourier transform, and the equation for the partial-wave radial wave function is found to be of the form [2]

$$u''_{l,j} + (p_i^2 \delta_{ij} - A_{ij}) u_{l,j} - B_{ij} u'_{l,j} = 0, \tag{3.10}$$

where A_{ij} contains the potential, nonlocal contributions, and the centrifugal barrier, while B_{ij} is only present when nonlocal contributions are included. This equation can be easily solved numerically using a method derived by Bergervoet [21]. A discussion of how to handle the presence of closed channels is given, for example, in Ref. [22]. As is well known, the inclusion of the Coulomb interaction in the configuration-space equation poses no additional complications.

The potentials are of such a form that they are exactly equivalent in both momentum space and configuration space. This means that the resulting phase shifts and mixing parameters are also the same, provided both equations (2.26) (in the static approximation) and (3.10) are solved with sufficient accuracy.

IV. MESONS, COUPLING CONSTANTS, AND FLAVOR SU(3)

A. The pseudoscalar mesons $J^{PC} = 0^{-+}$

In the literature one encounters two couplings for the pseudoscalar mesons to the $J^P = \frac{1}{2}^+$ baryons: the pseudoscalar coupling, $\mathcal{L}_{ps} = g\overline{\psi} i\gamma_5 \psi \phi$, and the pseudovector coupling, $\mathcal{L}_{pv} = (f/m_\pi)\overline{\psi}\gamma_5\gamma_\mu\psi\partial^\mu\phi$ (or a mixture of these two). We assume SU(3) for the pseudovector coupling f. Then, the Cabibbo theory of the weak interactions and the Goldberger-Treiman relation give $\alpha_{PV} = [F/(F+D)]_{pv} = 0.355$ [8]. In the Nijmegen soft-core models, this value could be imposed while still keeping an excellent description of the YN data, including the accurate datum on the capture ratio at rest.

The Nijmegen soft-core OBE models have quite sizable couplings to the baryons for the scalar ε meson (see below). If this were to be used in a model for the pion-nucleon interaction together with the pseudovector coupling for the pion, one would expect a large violation of the soft-pion constraints on the πN scattering lengths. However, the Nijmegen soft-core OBE models are compatible with these soft-pion constraints, because the potentially dangerous ε contribution is canceled by an opposite pomeron-exchange contribution [23].

B. The vector mesons $J^{PC} = 1^{--}$

An important ingredient of the baryon-baryon interaction is the exchange of the members of the vector-meson nonet (ρ, ϕ, ω, K^*). The details of our treatment of the vector mesons have been given in Refs. [24–26]; see also [27]. Ideal mixing between ω and ϕ implies

$\theta_V = 35.3°$, which means that the ϕ meson would be pure $s\bar{s}$, and hence would not couple to the nucleon. We assume a small deviation from ideal mixing and use the experimental value $\theta_V = 37.5°$ [8]. For the electric $F/(F+D)$ ratio we take $\alpha_V^e = 1$, as required by the "universality" assumption [9]. The magnetic α_V^m is not always the same. In the OBE models, the singlet-triplet strength in ΛN depends, besides on other things, especially on α_V^m. This feature is used to construct a range of soft-core models.

C. The scalar mesons $J^{PC} = 0^{++}$

The scalar mesons have constituted an important role in the construction of the Nijmegen potential models since 1970. They are an essential ingredient both in the hard-core models D [25] and F [26], and in all the soft-core models as well.

The scalar meson $\sigma(550)$ was introduced in 1960-1962 by Hoshizaki *et al.* [28]. In the OBE models for NN, this scalar meson was necessary for providing sufficient intermediate-range central attraction and for the spin-orbit interaction required to describe the ^3P_J splittings. In 1971 it was realized that the exchange of the broad $\varepsilon(760)$ could explain the role of the fictitious σ meson [29,30]. From then on, this broad $\varepsilon(760)$ has been used in the Nijmegen OBE models. A recent analysis of π production in πN scattering with polarized nucleons claimed to have found unambiguous evidence for a broad isoscalar $J^{PC} = 0^{++}$ state under the peak of the ρ meson [31]. This was based on an amplitude analysis involving besides π exchange also a_1 exchange in the production mechanism. In a similar analysis of data on $K^+n \to K^+\pi^-p$, evidence was found for an $I = \frac{1}{2}$, $0^+(887)$ strange scalar meson under the peak of the $K^*(892)$ meson [32]. In the latest issue of the Particle Data Group [33] this analysis is cited with reserve, asserting that the ε parameters of [31] cannot be correct because the $f_0(980)$ is neglected in the analysis.

Gilman and Harrari [34] showed that all Adler-Weisberger sum rules can be satisfied by saturation in the mesonic sector with the $\pi(140)$, $\varepsilon(760)$, $\rho(760)$, and $a_1(1090)$. They found the ε, in [34] called σ, to be degenerate with the ρ, having a width of $\Gamma(\varepsilon \to \pi\pi) =$ 570 MeV. Used in this work were the Regge high-energy behavior, SU(2)⊗SU(2) chiral algebra of charges, and pion dominance of the divergence of the axial-vector current. Similar phenomenology was derived by Weinberg requiring that the sum of the tree graphs for forward pion scattering, generated by a chiral-invariant Lagrangian, should not grow faster at high energies than permitted by Regge behavior of the actual amplitudes [35,36]. Therefore, it seems that chiral symmetry combined with Regge behavior requires a broad scalar ε degenerate with the ρ. Finally, we should mention that the Helsinki group now also finds an ε meson and other members of a scalar nonet [37].

In the quark model, the scalar mesons have been viewed as conventional $^3P_0$ $q\bar{q}$ states, while others view them as crypto-exotic $q^2\bar{q}^2$ states [38] or glueball states. We will briefly review the assignments as $q\bar{q}$ and as $q^2\bar{q}^2$ states.

In the $q\bar{q}$ picture, one has for the unitary singlet and octet states, denoted respectively by ε_1 and ε_8,

$$\begin{aligned} \varepsilon_1 &= \left(u\bar{u} + d\bar{d} + s\bar{s}\right)/\sqrt{3}, \\ \varepsilon_8 &= \left(u\bar{u} + d\bar{d} - 2s\bar{s}\right)/\sqrt{6}. \end{aligned} \tag{4.1}$$

The physical states are mixings of the pure SU(3) states and we write

$$\begin{aligned} \varepsilon &= \cos\theta_S \varepsilon_1 + \sin\theta_S \varepsilon_8, \\ f_0 &= -\sin\theta_S \varepsilon_1 + \cos\theta_S \varepsilon_8. \end{aligned} \tag{4.2}$$

Then, for ideal mixing we have $\tan\theta_S = 1/\sqrt{2}$ or $\theta_S \approx 35.3^\circ$, and so

$$\begin{aligned} \varepsilon &= f_0(760) = (u\bar{u} + d\bar{d})/\sqrt{2}, \\ f_0 &= f_0(980) = s\bar{s}. \end{aligned} \tag{4.3}$$

Note that in contrast to [2], we here follow for the description of the meson mixing the same conventions as for the pseudoscalar and vector mesons.

In the $q^2\bar{q}^2$ picture [38] (see also [27]), one introduces diquarks q^2 with $F = 3^*$, $C = 3^*$, and $S = 0$, for the flavor, color, and spin representations, respectively. Since $F = 3^*$, one denotes these diquark states by $\overline{Q}$. This conjugated triplet $\overline{Q}$ has the contents $\overline{S} = [ud]$, $\overline{U} = [sd]$, and $\overline{D} = [su]$, where $[ud]$ stands for the antisymmetric flavor wave function $ud - du$, and so on. The $Q\overline{Q}$ states form a scalar flavor nonet. In particular, Jaffe predicted the lowest-mass state (which we assume here to be ε) as $S\overline{S}$, with $I = 0$, $J^{PC} = 0^{++}$, and mass $M = 690$ MeV. In this scalar nonet, Jaffe predicted a degenerate pair of $I = 0$ and $I = 1$ state at $M = 1150$ MeV. It seems natural to identify these with the $f_0(980)$ and the $a_0(980)$. Explicitly, in the $q^2\bar{q}^2$ model, the quark content of the neutral states $f_0(760)$, $f_0(980)$, and $a_0(980)$ is

$$\begin{aligned} & S\overline{S} = [\bar{u}\bar{d}][ud], \\ & \left(U\overline{U} \pm D\overline{D}\right) = \left\{[\bar{s}\bar{d}][sd] \pm [\bar{s}\bar{u}][su]\right\}/\sqrt{2}. \end{aligned} \tag{4.4}$$

The strange members of this nonet are combinations like $\kappa^+ \sim [ud][\bar{s}\bar{d}]$, etc. These are expected at about $M = 880$ MeV, just under the $K^*(892)$. Ideal mixing in the case of the $q^2\bar{q}^2$ states means that

$$\begin{aligned} \varepsilon &= f_0(760) = S\overline{S}, \\ f_0 &= f_0(980) = (U\overline{U} + D\overline{D})/\sqrt{2}, \end{aligned} \tag{4.5}$$

which in this case implies that $\tan\theta_S = -\sqrt{2}$, or $\theta_S \approx -54.8^\circ$.

In view of the above, we note that ideal mixing for the scalar mesons in the case of $q^2\bar{q}^2$ states is quite distinct from that for the $q\bar{q}$ states. To analyze some of the differences between the $q\bar{q}$ and the $q^2\bar{q}^2$ assignments for the BB channels, we remind the reader that in our strategy we keep the NN channel fixed. Considering the mixing, one obtains for $g_{NN\varepsilon}$ and g_{NNf_0}, in terms of the flavor singlet and octet couplings,

$$\begin{aligned} g_{NN\varepsilon} &= \cos\theta_S g_1 + \sin\theta_S g_8, \\ g_{NNf_0} &= -\sin\theta_S g_1 + \cos\theta_S g_8, \end{aligned} \tag{4.6}$$

where $g_1 = g_{NN\varepsilon_1}$ and $g_8 = g_{NN\varepsilon_8} = (4\alpha_S - 1)g_{NNa_0}/\sqrt{3}$. Because g_{NNa_0}, $g_{NN\varepsilon}$, and g_{NNf_0} are fitted to the NN scattering data, the only freedom left for the YN and the YY systems is in the variation of the scalar mixing angle θ_S. The scalar $F/(F+D)$ ratio is restricted by

$$g_8 \equiv \frac{(4\alpha_S - 1)}{\sqrt{3}} g_{NNa_0} = \sin\theta_S g_{NN\varepsilon} + \cos\theta_S g_{NNf_0}, \tag{4.7}$$

from which it is clear that $\alpha_S = \alpha_S(\theta_S)$. This relation implies roughly that for positive values of θ_S we get $\alpha_S > 0$, while for negative values we get $\alpha_S < 0$. For the ideal mixing in the $q\bar{q}$ case $\alpha_S \approx +1.0$, and for ideal mixing in the $q^2\bar{q}^2$ case $\alpha_S \approx -1.0$. This difference between the $q\bar{q}$ and the $q^2\bar{q}^2$ assignment is quite important for the YN and the YY systems. In principle, one could of course allow for the possibility that the actual physical states, $\varepsilon(760)$ and $f_0(980)$, are mixtures of the $q\bar{q}$ and the $q^2\bar{q}^2$ states. We expect that $\theta_S > 0$ if the $q\bar{q}$ component dominates, whereas $\theta_S < 0$ when the $q^2\bar{q}^2$ component dominates.

In Fig. 1, we show the strength of the scalar-exchange central potential, in arbitrary units, for the diagonal matrix elements in YN. Here, we assumed equal masses for the members of the scalar nonet. Considering the contribution from the scalar nonet, we note the following. In the $\Sigma^+p(^3S_1)$ channel, the scalar-nonet contribution is attractive in the $q\bar{q}$ case, whereas in the $q^2\bar{q}^2$ case it is repulsive. Note that for the spin-singlet the interaction in ΛN is quite similar to that in ΣN, due to the dominance of the $\{27\}$ irrep. Although outside the scope of the present paper, we mention that in the $\Lambda\Lambda(^3S_1)$ channel the scalar-nonet contribution is much stronger for $q^2\bar{q}^2$ domination than for $q\bar{q}$ domination. A similar situation occurs for the $\Xi N(^1S_0, I = 0)$ and $\Xi N(^3S_1, I = 1)$ states. So far, the soft-core OBE models all have $\theta_S > 30°$, which indeed implies that the $\Lambda\Lambda$ and the ΞN potentials are rather weakly attractive in the intermediate range. They therefore cannot produce sufficient attraction to account for the binding energies of the experimentally found double-Lambda hypernuclei, e.g., ${}^{10}_{\Lambda\Lambda}\mathrm{Be}$ [39].

D. The pomeron $J^{PC} = 0^{++}$ and the heavy mesons

The physical nature of pomeron-exchange can be understood in the framework of QCD as a two-gluon (or multigluon) exchange effect. In the Low-Nussinov two-gluon model [40], it was once proposed [41] to distribute the two-gluon coupling over the quarks of a hadron, the so-called "subtractive pomeron". Then, one would expect at low energies an attractive van der Waals type of force. This is in conflict with the results from Regge phenomenology [3]. However, it became apparent experimentally in the study of the $pp \to (\Lambda\phi K^+)p$ and $pp \to (\Lambda\overline{\Lambda}p)p$ reactions at $\sqrt{s} = 63$ GeV [42,43] that the pomeron couples dominantly to individual quarks. This leads to the so-called "additive pomeron". The dominance of the one-quark coupling can be understood as due to the fact that in the case of a coupling to two quarks the loop momentum involved in such a coupling has to pass through at least one baryon. Thus, the baryon wave function is involved, which leads to a suppression of a^2/R^2 [44], where a and R are the quark and baryon radius, respectively. It is interesting to know whether this is also true at lower energies. In the Low-Nussinov model one can argue that the pomeron-quark coupling leads to a repulsive Gaussian potential [27], which has been used in the Nijmegen soft-core models. The importance of the pomeron in OBE models being compatible with chiral symmetry has already been mentioned above, see also [23].

Exact SU(3) and unitarity cause a strong mixing between the "bare" pomeron and the isosinglet member of the tensor mesons. Medium strong SU(3) breaking then gives mixing of these bare states, leading to the physical pomeron and f_2 tensor meson. This is why we include the $J = 0$ contributions from the tensor f_2, f_2', and a_2 Regge trajectories. So far, the explicit exchange of axial and tensor mesons has hardly been explored in models of baryon-baryon interactions for low energies. The axial mesons are very important in connection with chiral symmetry and play an important role in sum rules [45]. The tensor mesons are very important at higher energies, lying on a dominant Regge trajectory, and they are exchange-degenerate with the vector mesons. In principle, there is no problem in the present approach to incorporate these heavy mesons. (We already include the $J = 0$ contribution from the tensor mesons.) Recently, we have included these mesons explicitly, using the estimates based on the Regge hierarchy from [3] as a guidance for the coupling constants. With regard to the general features, no qualitative changes in the description of the NN and YN channels were observed. This can be understood from the fact that these mesons have masses well above 1 GeV, and hence are expected to affect the interaction only at very short distances. But the short-distance part of the interaction can already very well be parameterized phenomenologically by the form factor parameters at the BBM vertices.

V. BROKEN SU(3) FORM FACTORS AND COUPLING CONSTANTS

A. Form Factors

In this paper we describe the results of the NSC97 models where the form factors depend on the SU(3)$_F$ assignment of the mesons, rather than on the SU(3)$_F$-irrep structure of the BB channel. The latter was done for the NSC89 model [2]. In principle, we can introduce different form factor masses Λ_8 and Λ_1 for the $\{8\}$ and $\{1\}$ members of each meson nonet. However, for practical reasons, we neglect the finer details of the isoscalar octet and singlet meson mixing, and assign Λ_1 to the physical isoscalar mesons and Λ_8 to the physical octet mesons. At this stage we are not yet trying to limit the number of free parameters to an absolute minimum, and so here we also introduce a separate parameter Λ_K for the strange mesons. For example, for the pseudoscalar mesons we have the following cut-off parameters: Λ_1 for the $BB\eta'$ vertices, Λ_8 for the $BB\pi$ and $BB\eta$ vertices, and Λ_K for the BBK vertices.

B. BBM coupling constants

For the flavor-symmetry breaking of the coupling constants we use the $^3P_0$ mechanism [7,13] for the meson-baryon-baryon coupling. In the $^3P_0$ model, which is rather successful for meson decay [46], the BBM coupling is due to the rearrangement of the quark of a virtual quark-antiquark pair in the vacuum and a valence quark in the baryon. Such a rearrangement leads the initial baryon state into the final baryon-meson state. The amplitude for the formation of a meson is calculated from the overlap between the wave functions of the incoming baryon, the outgoing baryon, the outgoing meson, and the $q\bar{q}$-pair wave function. For reasons of simplicity it is usually assumed that the momentum distribution of the created pair is independent of the momenta.

In scattering, one has to describe not only the emission of mesons, but also the absorption of mesons. In a Feynman graph a single vertex implicitly contains both processes and there is no distinction between emission and absorption. Consider now the ΛNK vertex as a specific example. In the quark model the emission of a K is described by the creation of a non-strange $q\bar{q}$ pair, whereas the absorption of a K is described by the annihilation of an $s\bar{s}$ pair. To implement SU(3)$_F$-symmetry breaking within the context of the $^3P_0$ model, the usual $^3P_0$ interaction for decay has to be generalized. In [13] this is done by introducing a factor which describes the transition of a quark from within a baryon to a quark within a meson, or vice versa. This symmetric treatment of the "moving" quarks and the pair quarks then leads to a covariant vertex. Therefore, in [13] the $^3P_0$ Hamiltonian for the BBM couplings is taken as follows

$$H_I = \int d^3x \int d^3y F(x-y)\,[\bar{q}(x)O_{\bar{q}q}q(x)]^{(1)} \otimes [\bar{q}(y)O_{\bar{q}q}q(y)]^{(2)}\,, \tag{5.1}$$

where the quark-field operators are vectors in flavor space, with components $q_i = (u, d, s)$ and $\bar{q}_i = (\bar{u}, \bar{d}, \bar{s})$. In Eq. (5.1) it is understood that the first factor creates or annihilates a $q\bar{q}$ pair, whereas the second factor "moves" a quark from the baryon into the meson or vice versa. The operator $O_{\bar{q}q}$ is a matrix in quark-flavor space which is diagonal if we assume there is no quark mixing. Since in general it will break SU(3) and SU(2) symmetry, it will be of the form

$$(O_{\bar{q}q})_{i,j} = \begin{pmatrix} \gamma_u & 0 & 0 \\ 0 & \gamma_d & 0 \\ 0 & 0 & \gamma_s \end{pmatrix}, \tag{5.2}$$

where the pair-creation constants γ_u, γ_d, and γ_s are unequal.

The space-time structure will not play an important role in this paper. We assume that the effects from the overlap of the wave functions can be effectively absorbed into the γ constants. Hence, our matrix elements will contain an SU(2)$_S$ part due to the spins, and an SU(3)$_F$ part due to the flavors, and so from here on we can restrict ourselves to deal explicitly only with the spin and flavor part of the interaction Hamiltonian density.

Writing the O_{ij} matrix elements in terms of the SU(3) generators $F_i = \lambda_i/2$, $(i = 1, \ldots, 8)$, where λ_i are the well-known Gell-Mann matrices, we have

$$O_{\bar{q}q} = \gamma_0 F_0 + \gamma_3 F_3 + \gamma_8 F_8, \tag{5.3}$$

with F_0 the unit matrix. We neglect isospin breaking of the coupling constants, and we set $\gamma_u = \gamma_d \equiv \gamma_n$. This gives

$$\gamma_0 = \frac{1}{3}(2\gamma_n + \gamma_s), \quad \gamma_3 = 0, \quad \gamma_8 = \frac{2}{\sqrt{3}}(\gamma_n - \gamma_s). \tag{5.4}$$

For $\gamma_u = \gamma_d = \gamma_s$ one has exact SU(3)$_F$ symmetry, assuming there is no breaking due to differences between the wave functions of different quark flavors. For $\gamma_u = \gamma_d \neq \gamma_s$, one gets a breaking of the coupling constants. In this case, there is still isospin symmetry, SU(2)$_I$, but SU(3)$_F$ is broken. As an operator in flavor space, the interaction (5.1) can now be written as

$$\begin{aligned} \mathcal{H}_I &= [\gamma_0 F_0 + \gamma_8 F_8]^{(1)} \otimes [\gamma_0 F_0 + \gamma_8 F_8]^{(2)} \\ &= \mathcal{H}_I^{(1)} + \mathcal{H}_I^{(8)} + \mathcal{H}_I^{(8\otimes 8)}, \end{aligned} \tag{5.5}$$

where the singlet interaction, $\mathcal{H}_I^{(1)}$, and the octet interaction, $\mathcal{H}_I^{(8)}$, correspond to the γ_0^2 and $\gamma_0\gamma_8$ terms, respectively. Because we expect that the SU(3)$_F$ symmetry is not broken by more than 20%, the $8 \otimes 8$ interaction as given by the γ_8^2 term will be rather small. In the $^3P_0$-model calculations [13] the $8 \otimes 8$ piece is implicitly included and can readily be retrieved from the results by translating γ_n and γ_s into γ_0 and γ_8.

The $^3P_0$ model has approximately SU(6)$_W$ symmetry [47]. Therefore, in [13] the BBM couplings were evaluated using SU(6)$_W$ wave functions. Since in SU(6)$_W$ the majority of the mesons have $W = 1$, we use here the results for the SU(3)$_F$ breaking for $W = 1$ for all mesons. In terms of the SU(3)-flavor breaking parameter $\lambda_{\rm fsb} = \gamma_s/\gamma_n$, the modification to the pseudovector coupling constants is as follows. For the K,

$$
\begin{aligned}
f_{\Lambda NK} &\rightarrow f_{\Lambda NK} - f_{\Lambda NK}(1-\lambda_{\rm fsb}),\\
f_{\Lambda \Xi K} &\rightarrow f_{\Lambda \Xi K} - f_{\Lambda \Xi K}(1-\lambda_{\rm fsb}),\\
f_{\Sigma NK} &\rightarrow f_{\Sigma NK} - f_{\Sigma NK}(1-\lambda_{\rm fsb}),\\
f_{\Sigma \Xi K} &\rightarrow f_{\Sigma \Xi K} - f_{\Sigma \Xi K}(1-\lambda_{\rm fsb}),
\end{aligned}
\tag{5.6}
$$

for the η_8,

$$
\begin{aligned}
f_{\Sigma\Sigma\eta_8} &\rightarrow f_{\Sigma\Sigma\eta_8} - \tfrac{1}{3} f_{\Sigma\Sigma\eta_8}(1-\lambda_{\rm fsb}^2),\\
f_{\Xi\Xi\eta_8} &\rightarrow f_{\Xi\Xi\eta_8} - \tfrac{8}{9} f_{\Xi\Xi\eta_8}(1-\lambda_{\rm fsb}^2),
\end{aligned}
\tag{5.7}
$$

and for the η_0,

$$
\begin{aligned}
f_{\Lambda\Lambda\eta_0} &\rightarrow f_{\Lambda\Lambda\eta_0} - f_{\Lambda\Lambda\eta_0}(1-\lambda_{\rm fsb}^2),\\
f_{\Sigma\Sigma\eta_0} &\rightarrow f_{\Sigma\Sigma\eta_0} + \tfrac{1}{3} f_{\Sigma\Sigma\eta_0}(1-\lambda_{\rm fsb}^2),\\
f_{\Xi\Xi\eta_0} &\rightarrow f_{\Xi\Xi\eta_0} - \tfrac{4}{3} f_{\Xi\Xi\eta_0}(1-\lambda_{\rm fsb}^2).
\end{aligned}
\tag{5.8}
$$

Similar expressions apply for the vector and scalar mesons.

VI. FIT TO *YN* TOTAL CROSS SECTIONS

In principle, the potential model contains four free parameters for each type of meson exchange, and (at this stage) three cut-off parameters to regularize the corresponding baryon-baryon-meson vertices. As mentioned earlier, the advantage of abandoning the SU(3)-irrep scheme for the cut-off parameters is that now the fit to the YN (and NN) scattering data fixes all parameters, and so the model can be readily extended to the strangeness $S = -2$, -3, and -4 sectors. The SU(3)-irrep scheme requires the introduction of new cut-off parameters for these channels, whereas there are no experimental data to fix them.

We have made six different fits to the YN scattering data, including partial waves up to $L = 2$. The data we use are tabulated in Ref. [2], and are at sufficiently low energies that the contributions of the higher partial waves can be safely neglected. The NN interaction puts constraints on most of the parameters, and so we are left with only a limited set of parameters that we can vary. The parameters common to all six models are given in Table II. For the remaining parameters we chose six fixed values for the magnetic vector-meson $F/(F+D)$ ratio α_V^m, ranging from $\alpha_V^m = 0.4447$ to $\alpha_V^m = 0.3647$. Adjusting the scalar mixing angle θ_S and the SU(3)-flavor breaking parameters $\lambda_{\rm fsb}$, equally good fits to the YN scattering data have been obtained. The fitted parameters are given in Table III, where the models NSC97a through NSC97f are classified by their different choices for the magnetic vector-meson $F/(F+D)$ ratio α_V^m.

The aim of the present study is to construct a set of models which give essentially the same fit to the YN scattering data, but which differ somewhat in the details of their parameterization. These models will then be used to study the model dependence in calculations of hypernuclei and in their predictions for the $S=-2$, -3, and -4 sectors. Especially for the latter application, these models will be the first models for the $S<-1$ sector to have their theoretical foundation in the NN and YN sectors. The results for the $S<-1$ sector will be presented in a future publication.

The χ^2 on the 35 YN scattering data for the different models is given in Table IV. Although there is some variation in the description of some experiments from one model to the next, these variations are rather small. The total χ^2 on all data varies only a little, and is found to be 15.68, 15.82, 15.62, 15.76, 16.06, and 16.67, for models NSC97a through NSC97f, respectively. The capture ratio at rest, given in the last column of Table IV, is defined as

$$r_R = \frac{1}{4}\,\frac{\sigma_s(\Sigma^-p\rightarrow\Sigma^0 n)}{\sigma_s(\Sigma^-p\rightarrow\Lambda n)+\sigma_s(\Sigma^-p\rightarrow\Sigma^0 n)} + \frac{3}{4}\,\frac{\sigma_t(\Sigma^-p\rightarrow\Sigma^0 n)}{\sigma_t(\Sigma^-p\rightarrow\Lambda n)+\sigma_t(\Sigma^-p\rightarrow\Sigma^0 n)}, \tag{6.1}$$

where σ_s is the total reaction cross section in the singlet ${}^1S_0$ partial wave, and σ_t the total reaction cross section in the triplet-coupled ${}^3S_1$-${}^3D_1$ partial wave, both at zero momentum. In practice these cross sections are calculated at $p_{\rm lab}=10$ MeV/c, which is close enough to zero. The capture ratio at nonzero momentum is the capture ratio in flight, defined as

$$r_F = \frac{\sigma(\Sigma^-p\rightarrow\Sigma^0 n)}{\sigma(\Sigma^-p\rightarrow\Lambda n)+\sigma(\Sigma^-p\rightarrow\Sigma^0 n)}. \tag{6.2}$$

This capture ratio turns out to be rather constant up to lab momenta of about 150 MeV/c. Obviously, for very low momenta the cross sections are almost completely dominated by S waves, and so the capture ratio in flight converges to the capture ratio at rest.

The comparison to the experimental data for models NSC97a, NSC97c, and NSC97f is shown in Fig. 2. Models NSC97b, NSC97d, and NSC97e give similar results, but are left out to avoid overcrowding in the figures. The Λp total cross section in Fig. 2(b) shows a pronounced cusp of almost 50 mb at the Σ^+n threshold, which is caused by the coupling of the ΛN and ΣN channels and the rather strong interaction in the ${}^3S_1$-wave ΣN channel. Because the cusp occurs over a very narrow momentum range, it is hard to see this effect experimentally. Indeed, the old bubble-chamber data [53,54] have too large error bars to identify any possible cusp effect. (Note that these data have not been used in our fits.)

It should be noted that the Σ^+p and Σ^-p elastic cross sections are not the "true" total cross sections. The latter are hard to measure because of the large Coulomb contribution at forward angles. The cross sections that were measured are defined as [50]

$$\sigma = \frac{2}{\cos\theta_{\rm max}-\cos\theta_{\rm min}}\int_{\theta_{\rm min}}^{\theta_{\rm max}}\frac{d\sigma(\theta)}{d\cos\theta}d\cos\theta, \tag{6.3}$$

with typical values -0.2 to -0.5 for $\cos\theta_{\rm min}$ and 0.3 to 0.5 for $\cos\theta_{\rm max}$. In order to stay as close as possible to the plotted experimental data, the theoretical curves in Figs. 2(c) and (d) have been calculated with $\cos\theta_{\rm min} = -0.5$ and $\cos\theta_{\rm max} = 0.5$. The Heidelberg group [50] also presents elastic differential cross sections for $\Sigma^{\pm}p$ scattering at $p_{\Sigma^{\pm}} = 170$ and 160 MeV/c, respectively. The corresponding potential model predictions are plotted in Fig. 3; again, only models NSC97a, NSC97c, and NSC97f are shown.

Although the six models give an equally good description of the (few) YN scattering data, the different choices for α_V^m give rise to different properties on a more detailed level. This implies that these scattering data do not unambiguously determine the YN interaction. For example, in Fig. 4 we show the wide spread in the Λp $^1S_0$ and Σ^+p $^3S_1$ phase shifts which, according to the results in Table IV, are still compatible with the scattering data. Also, the S-wave scattering lengths in the four YN channels exhibit a fair amount of variation from one model to the next, as shown in Table V.

As will be discussed in the next section, the differences among these models in applications other than low-energy YN scattering are even more pronounced. As a consequence, they will provide important information to further pin down the YN interaction. It is found that especially NSC97f exhibits nice features when applied to hypernuclear systems. Therefore, rather than providing many tables with results for all the models, we will here only give some results for NSC97f. The phase shifts for Σ^+p and Λp scattering are given in Tables VI and VII, respectively. Predictions for the total cross sections in the Λp channel above the ΣN thresholds are given in Table VIII, while those for the total nuclear (i.e., without Coulomb) cross sections in the Σ^-p channel are given in Table IX.

VII. G-MATRIX ANALYSES OF NSC97 MODELS

The properties of hypernuclear systems are linked closely to the underlying YN interactions. Since the free-space YN scattering data are sparse at the present stage, it is quite important to test our OBE models through the study of hypernuclear phenomena. Especially, the coming precise data of γ-ray observation from Λ hypernuclei will provide very valuable information on the spin-dependent forces such as spin-spin and spin-orbit interactions. Effective YN interactions in a nuclear medium, which reflect the properties of the bare interactions, can be derived using the G-matrix procedure. One of the authors (Y.Y.) and his collaborators performed the G-matrix calculations in nuclear matter with the various OBE models by the Nijmegen [25,26,2] and Jülich groups [55,56], and found specific differences among them [57,4,58]. Here, we discuss the properties of G-matrix interactions derived from the NSC97 models in comparison with the old NSC89 version [2], and the hard-core models D [25] and F [26] (referred to as NHC-D and NHC-F, respectively). In order to compare the present results with the past works [57,4,58], the calculations are done in the same framework: We adopt the simple QTQ prescription for the intermediate-state spectrum, which means that no potential term is taken into account in the off-shell propagation. As discussed later, this procedure is reliable enough to investigate the feature of spin-dependent terms.

In Table X we show the potential energies U_Λ for a zero-momentum Λ and their partial-wave contributions $U_\Lambda(^{2S+1}L_J)$ at normal density (k_F=1.35 fm^{-1}) for the NSC97 models, where a statistical factor $(2J+1)$ is included in $U_\Lambda(^{2S+1}L_J)$. It is seen that the values for each state vary smoothly from NSC97a to NSC97f. The obtained values for U_Λ are not so far from the well depths (∼28 MeV) of Λ-nucleus Woods-Saxon potentials as obtained from analyses of the (π^+, K^+) reaction data [59–61], though the comparison should be only considered on a qualitative level. It should be noted here that the odd-state interactions, which are uncertain experimentally, are very different among the various OBE models. In the case of the NSC97 models, the odd-state contributions are found to be strongly repulsive. On the other hand, they are strongly attractive, weakly attractive, and almost vanishing in the case of NHC-D, NHC-F, and NSC89, respectively [58]. The stronger odd-state repulsion of the NSC97 models is compensated by the also stronger even-state attraction.

It is noted that the relative ratios of $U_\Lambda(^1S_0)$ and $U_\Lambda(^3S_1)$ are very different among the NSC97 models, as seen in Table X, indicating different spin-spin interactions. In order to see the spin-dependent features of the G-matrix interactions more clearly, we obtain the contributions to U_Λ from the spin-independent, spin-spin, LS, and tensor components of the G matrices, denoted as U_0, $U_{\sigma\sigma}$, U_{LS}, and U_T, respectively, by the following transformations:

$$\begin{aligned}
U_0(S) &= \frac{1}{4}\left\{U(^3S_1)+U(^1S_0)\right\}, \\
U_{\sigma\sigma}(S) &= \frac{1}{12}\left\{U(^3S_1)-3U(^1S_0)\right\}, \\
U_0(P) &= \frac{1}{12}\left\{U(^3P_0)+U(^3P_1)+U(^3P_2)+3U(^1P_1)\right\}, \\
U_{\sigma\sigma}(P) &= \frac{1}{36}\left\{U(^3P_0)+U(^3P_1)+U(^3P_2)-9U(^1P_1)\right\}, \\
U_{LS}(P) &= \frac{1}{12}\left\{-2U(^3P_0)-U(^3P_1)+U(^3P_2)\right\}, \\
U_T(P) &= \frac{1}{72}\left\{-10U(^3P_0)+5U(^3P_1)-U(^3P_2)\right\}. \qquad (7.1)
\end{aligned}$$

The obtained values are shown in Table XI, where also the ones for NSC89, NHC-D, and NHC-F are given for comparison. We can see here the nice correlation between the α_V^m values taken in the NSC models and the strengths of the spin-spin interactions in even states; the smaller value of α_V^m leads to the more repulsive strength. This marked difference of the spin-spin interactions for NSC97a–f will show up characteristically in hypernuclear spectra, which should be tested in comparison with experimental data. On the other hand, the differences of LS components amongst the Nijmegen models turn out to be less remarkable than the spin-spin ones. It is notable here that also the strengths of the LS interactions vary smoothly with the α_V^m values in the NSC97 models. The detailed discussion of spin-orbit components is given later.

As is well known, there remains some ambiguity in the lowest-order G-matrix approximation concerning the intermediate spectrum in the propagator. The choice of a continuous intermediate-energy spectrum (CIES), extended smoothly from the on-shell one, leads to the considerable gain of U_Λ values in comparison with the QTQ prescription [4,58,62]. Now, let us demonstrate that the spin-dependent parts are not so much affected by these different treatments, in spite of the considerable change of the spin-independent part U_0. In Table XII the above-defined components for NSC97f are compared for the cases of QTQ and CIES, where the results are given at $k_F = 1.35$ and $1.0\ \mathrm{fm}^{-1}$. It should be noted here that the differences of the spin-dependent parts are far smaller than those of the spin-independent ones U_0, especially in the case of $k_F = 1.0\ \mathrm{fm}^{-1}$. The reason is that these spin-dependent contributions are determined essentially by the differences of the partial-wave contributions, and the induced changes cancel out considerably. In addition, the P-state contributions are far less sensitive to the treatment of the intermediate spectrum than the S-state ones. Due to the same reasons, the density dependencies of the spin-dependent parts are considerably weaker than those of the spin-independent parts.

If the nucleon rearrangement effect is taken into account [57], the values of U_Λ are multiplied by $(1-\kappa_N)$, $\kappa_N = 0.10 \sim 0.15$ (at normal density) being the average correlation probability for nucleons. In Table XII we find that the QTQ results without the $(1-\kappa_N)$ correction simulate roughly the CIES results with this correction.

Thus, we can say that the G-matrix interactions are reliable enough for bridging the spin-dependent terms of the OBE models with hypernuclear spectra separately from the ambiguities of the spin-independent parts alluded to above. A convenient approach is, for instance, to adjust the spin-independent parts adequately so as to reproduce the experimental Λ binding energies in applying the G-matrix interactions to structure calculations of hypernuclei [58].

Let us discuss the Λ ℓ-s potentials in hypernuclei, which are derived from the LS and anti-symmetric LS (ALS) components of our G-matrix interactions, in comparison with the corresponding nucleon one. In the Scheerbaum-approximation [63] the ℓ-s potential is related to the two-body LS (ALS) interaction as follows:

$$\begin{aligned}
&U_B^{ls}(r) = K_B \frac{1}{r}\frac{d\rho}{dr}\,\mathbf{l}\cdot\mathbf{s} \qquad \text{with} \quad B = N, \Lambda, \\
&K_N = -\frac{\pi}{2} S_{LS} \quad \text{and} \quad K_\Lambda = -\frac{\pi}{3}(S_{LS} + S_{ALS}), \\
&S_{LS,ALS} = \frac{3}{\bar{q}} \int_0^\infty r^3 j_1(\bar{q}r)\, G_{LS,ALS}(r)\, dr,
\end{aligned} \tag{7.2}$$

where $G_{LS}(r)$ and $G_{ALS}(r)$ are the LS and ALS parts of the G-matrix interactions in configuration space, respectively, and $\rho(r)$ is the nuclear density distribution. We take here $\bar{q} = 0.7\ \mathrm{fm}^{-1}$ simply in the same way as [63], since the results are insensitive to the value of $\bar{q}$.

Table XIII shows the values of K_Λ and $S_{LS,ALS}$ obtained from the LS and ALS parts of the ΛN G-matrix interactions derived from various Nijmegen models, where the G matrices are calculated at $k_F = 1.0\ \mathrm{fm}^{-1}$. Due to the reason mentioned above, the LS and ALS parts are very insensitive to k_F. For comparison we give also K_N and S_{LS} for a typical NN G-matrix interaction ($G0$) [64] derived from the Reid soft-core potential. Here, it should be noted that the effective strengths S_{LS} of the ΛN LS interactions are not so small compared to that of NN. In the case of NSC97f, for instance, the absolute value of S_{LS} is smaller than that of NN by 66%, but the K_Λ value is smaller than the K_N one by 32%. There are two reasons why the values of K_Λ become so small compared to that of K_N. One is that K_Λ is smaller than K_N kinematically by 2/3, which is determined by the ratio of the number of NN and ΛN ^{3}O-bonds in the nucleus. The other reason is that the LS contribution is canceled substantially by the ALS one in the ΛN case.

Furthermore, be aware that the ratio of the Λ and N ℓ-s splitting energies should be further reduced compared with K_Λ/K_N. First, the value of K_N obtained with $G0$ accounts for only about 60 $\sim$ 70% of the empirical ℓ-s splitting; the additional contributions are supposed to come from the many-body correlations related to the Pauli exclusion effect [65], which are not expected to be present for a Λ particle. Second, the Λ single-particle wave function should extend farther than the N one due to its smaller binding energy, which leads to a reduction of the ΛN matrix elements. In the case of ${}^{17}_{\Lambda}$O, for instance, it was found that the Λ ℓ-s splitting energy evaluated with the precise Λ wave function is reduced by $\sim$ 25% from that with the single harmonic oscillator one [66]. Then, the ratio of Λ and N ℓ-s splitting energy is estimated as about one half of K_Λ/K_N. Precise calculations of Λ splitting energies can be done with use of the above values of K_Λ or $G_{LS,ALS}(r)$ themselves [66].

Thus, it is concluded that Λ ℓ-s splitting energies in hypernuclei are likely to be very small compared to nucleon ones, even if the ΛN LS interaction is not so much weaker than the NN one. Precise measurements of Λ ℓ-s splitting energies are crucially important to extract information on the two-body LS and ALS interactions.

Finally, we comment on the properties of the ΣN G-matrix interactions. The calculations are done in the same way as in Ref. [58]. The QTQ spectra are adopted in ΣN intermediate states, but continuous intermediate ones are taken into account in ΛN states coupled to ΣN channels. The potentials in the intermediate ΛN states only slightly influence the real parts of the ΣN G matrices, but work decisively on their imaginary parts related to the conversion width in nuclear matter. The reason is that the imaginary part is determined by the energy-conserving transition from the starting ΣN state to the ΛN one. We calculate here Σ single-particle potentials U_Σ and conversion widths Γ_Σ for the NSC97 models. The obtained results are more or less similar to each other. In Table XIV the calculated values of U_Σ and Γ_Σ at $k_F = 1.0$ fm^{-1} for the NSC97e and NSC97f are compared with those for the other Nijmegen models. We find remarkable differences among the models.

The Γ_Σ directly reflects the strength of the ΣN-ΛN coupling interaction, and those of the NSC97 models turn out to be considerably smaller than for NSC89. It is worthwhile to say that the moderate ΣN-ΛN coupling interactions of the NSC97 models are free from possible troubles which appear in applications of the NSC89 model to hypernuclear systems due to its too strong ΛN-ΣN coupling.

Recently, the existence of ${}^{4}_{\Sigma}$He has been confirmed [67], which gives valuable information on the ΣN interaction. The observed values of the Σ binding energy, B_Σ, and the width are $4.4 \pm 0.3 \pm 1$ MeV and $7.7 \pm 0.7^{+1.2}_{-0.0}$ MeV, respectively. As discussed in Ref. [68], the strong spin-isospin dependence shows up in the ΣN interaction, and the value of B_Σ is determined mainly by the attractions in the $T = 1/2\ {}^3S_1$ and $T = 3/2\ {}^1S_0$ states. It should be noted that the NSC97 models are adequately attractive in these states, as well as the other Nijmegen models. Be careful that our calculated values of Γ_Σ should not be compared directly to the above experimental one. Because of weak binding of the Σ, the wave function extends outwards and is of small overlap with the nucleon ones, which leads likely to a remarkable reduction of Γ_Σ. It is an open problem to perform exact four-body calculations on the basis of these OBE models.

VIII. DISCUSSION AND OUTLOOK

The NSC97 models are an important step forward in the realization of a program where the baryon-baryon interactions for scattering and hypernuclei can be described in the context of broken $SU(3)_F$ symmetry.

First, it turns out that starting from the soft-core OBE model for NN, we are indeed able to achieve a very good description of the YN data and at the same time maintain values for the free parameters which are consistent with the present view on low-energy hadron physics. For example, the value used for the $F/(F+D)$ ratio α_{PV} for the pseudoscalar mesons is the same as that found in the weak interactions; see, e.g., Ref. [8]. Also, the range of values used for the magnetic ratio of the vector mesons is compatible with the estimates from static and non-static SU(6) [10].

Second, for the first time the soft-core model NSC97f passes the tests from the hypernuclear studies very satisfactorily. It is no longer necessary to introduce a phenomenological spin-spin interaction for the ΛN systems, as was the case for the NSC89 model [2], see Ref. [4]. This is an important achievement with the NSC97 models.

Third, the NSC97 models give parameter-free predictions for the $S = -2, -3, -4$ two-body systems. In the $S = -2$ systems, the experimental information is limited to the ground states of ${}_{\Lambda\Lambda}^{6}\mathrm{He}$, ${}_{\Lambda\Lambda}^{10}\mathrm{Be}$, and ${}_{\Lambda\Lambda}^{13}\mathrm{B}$, from which it is inferred that $\Delta B_{\Lambda\Lambda} = 4 - 5$MeV, corresponding to a rather strong attractive $\Lambda\Lambda$ interaction. The estimate for the ${}^1S_0$ $\Lambda\Lambda$ matrix element in ${}_{\Lambda\Lambda}^{6}\mathrm{He}$ for NHC-D [25] is $\Delta B_{\Lambda\Lambda} = 4$ MeV, in agreement with the experimental observation. For more details we refer to Ref. [58]. Now, the characteristic feature of NHC-D is that, instead of a scalar nonet, there is only a scalar singlet. This makes the scalar central attraction independent of the baryon-baryon channel, and hence equally strong as in NN. However, in the soft-core models constructed sofar, we have nearly ideal mixing for $q\bar{q}$ states, which implies that

$$|V_{\Lambda\Lambda}(0^+)| < |V_{\Lambda N}(0^+)| < |V_{NN}(0^+)|,$$

which leads to much weaker attractive potentials than in the case of NHC-D in the $\Lambda\Lambda$ and ΞN systems. For example, an estimate for the $\Lambda\Lambda({}^1S_0)$ scattering length, based on $\Delta B_{\Lambda\Lambda}$ quoted above, is $a_{\Lambda\Lambda}({}^1S_0) \approx -2.0$ fm [69,70]. In the NSC97 models we obtain values between –0.3 and –0.5 fm. The only way to produce stronger $\Lambda\Lambda$ forces is to go to smaller θ_S and ipso facto a smaller α_S. However, when we tried this for the soft-core OBE models, we produced a $\Lambda N({}^1S_0)$ bound state. On the other hand, preliminary results from a potential model which includes also the two-meson-exchange contributions within the present framework, do show the apparently required attraction in the $\Lambda\Lambda$ interaction. This model is currently under further development.

Finally, to put the NSC97 models in perspective, we conclude by discussing the present situation of the Nijmegen models for the central, spin-spin, and spin-orbit interactions with respect to information from hypernuclear studies.

1. Central interaction

The Λ well depth U_Λ in nuclear medium is of basic importance in hypernuclear physics. The data of the middle and heavy Λ hypernuclei at BNL [60] and KEK [61] play an essential role, because it seems rather ambiguous to extrapolate U_Λ from Λ binding energies in light systems. The phenomenological analyses that have been performed for experimental B_Λ values with the use of Woods-Saxon potentials, indicate a depth of $\sim$ 28 MeV [59,61]. Some OBE models, including the present NSC97 ones, reproduce this value fairly well in the lowest-order G-matrix theory. From a fundamental many-body point of view, however, the comparison should be considered as being qualitative, because of ambiguities in this G-matrix approximation, especially in the spin-independent parts. One of the features of NSC97 models is that the odd-state interactions are strongly repulsive, but are compensated by the strong even-state attractions. This in contrast to the earlier Nijmegen models. It is an open problem to test this feature, for instance, by analyzing the experimental Λ single-particle spectra in medium and heavy hypernuclei [58].

2. Spin-spin interaction

The spin-doublet splittings ($J_{>,<} = J_c \pm s^\Lambda_{1/2}$) of several hypernuclei have been analyzed extensively by Yamamoto *et al.* [58] using the G-matrix interactions derived from the Nijmegen and Jülich potentials. As seen in Table XI, the strengths of the spin-spin interactions are very different among the Nijmegen models, where the most repulsive (attractive) is that of NSC89 (NHC-D). Those of the Jülich potentials are known to be more attractive than NHC-D [58]. The spin-spin interactions show up in the differences of the $^1S_0$ and $^3S_1$ phase shifts. The values obtained for Λp scattering at $p_\Lambda = 200$ MeV/c are $-18.89°$, $-15.33°$, $-10.55°$, $-3.34°$, $1.40°$, $5.60°$, $9.14°$, $-4.17°$, and $2.02°$ for NSC97 models a, b, c, d, e, f, NSC89, NHC-D, and NHC-F, respectively. Here, positive (negative) values mean repulsive (attractive) spin-spin interactions. Comparing these values to those for $U_{\sigma\sigma}$, we find a nice systematic correspondence between them. The experimental manifestation of the ΛN spin-spin interaction is found in the 0^+-1^+ doublet states of $^4_\Lambda$H and $^4_\Lambda$He [71], where the $J_< = 0^+$ state is below the $J_> = 1^+$ one by about 1 MeV. The analysis of $^4_\Lambda$H with the G-matrix interactions indicates that the spin-spin interaction should be repulsive and its adequate strength is between those of NHC-F and NSC89 [58]. Then, that of NSC97e or NSC97f seem to be of adequate strength, though a definite conclusion should be based on more elaborate four-body calculations. A complementary indication can be obtained from the exact three-body calculations of $^3_\Lambda$H by Miyagawa *et al.* [72,73], where the repulsive (attractive) spin-spin interaction of NSC89 (Jülich A) is shown to be adequate (inadequate) to reproduce the experimental Λ binding energy. Recently, Miyagawa performed the same calculations using the NSC97 models [74]: The model NSC97f, whose spin-spin interaction is of the most repulsive among the NSC97 models, reproduces a reasonable Λ binding energy. On the other hand, the model NSC97e gives rise to only a very weakly bound state compared to the experimental one, and no bound states are obtained for models NSC97a–d. Thus, the $^3_\Lambda$H problem turns out to be one of the critical tests for the spin-spin interactions.

Results for the NSC97 potentials with regard to the Carlson-Gibson computation [75] of the ${}^3_\Lambda$He, ${}^4_\Lambda$He, and ${}^5_\Lambda$He hypernuclei are not available yet.

The ground-state doublet splitting energies of some light p-shell hypernuclei are also indicative of the spin-spin interactions. The shell-model analyses of ${}^{10}_{\Lambda}$B, ${}^{11}_{\Lambda}$B, ${}^{12}_{\Lambda}$C, and ${}^{12}_{\Lambda}$B with the G-matrix interactions showed that the repulsive spin-spin interactions such as NHC-F and NSC89 make the $J_<$ states lower than the $J_>$ states [58]. (Experimentally the ground-state spins of ${}^{11}_{\Lambda}$B and ${}^{12}_{\Lambda}$B are $J_< = 5/2^+$ and 1^-, respectively.) This situation is altered by the LS and ALS interactions, however, which works more attractively on the $J_>$ states against the spin-spin interaction. For instance, the spin-spin interaction of NHC-F is weakly repulsive and makes $J_<$ states slightly lower than $J_>$ states, but this order is reversed by adding the LS and ALS terms [58]. On the other hand, the spin-spin interaction of NSC89 is so repulsive that the $J_<$ states are kept lower [58]. Although the spin-spin interaction of NSC97f is less repulsive than that of NSC89, the $J_<$ states are also kept lower, in spite of adding the LS and ALS ones [76]. Considering that the spin-spin interaction of NSC89 is suggested to be too repulsive [58], that of NSC97f is expected to be of reasonable strength. The less repulsive one of NSC97e is maybe of lower limit. Of course, there still remain ambiguities because the strengths of LS and ALS interactions are not established experimentally.

As new experiments are planned using hypernuclear γ-ray spectrometers with the germanium detectors [77], there are good prospects for progress in this sector. For instance, the planned experiment of the ground-state doublet splitting of ${}^7_\Lambda$Li is very promising, because this splitting is considered to be fairly free from the LS and ALS interactions [78]. In contrast, the $[{}^8\mathrm{Be}(2^+) \otimes (s_{1/2})_\Lambda]_{5/2^+,3/2^+}$ splitting in ${}^9_\Lambda$Be is almost purely determined by the LS and ALS interactions [78]. In view of these developments, one can envisage that the ΛN spin-spin and spin-orbit interactions will be established rather well in the coming years.

3. Spin-orbit interaction

The Λ ℓ-s splitting energies in hypernuclei are related intimately to the two-body LS and ALS components of ΛN interactions. It has been observed that the Λ ℓ-s splitting energies are far smaller than the nucleon ones. The first indication was given by the ${}^{16}\mathrm{O}(K^-,\pi^-){}^{16}_{\Lambda}\mathrm{O}$ experiment at CERN [79]. The splitting of the observed two peaks of the $[(p^{-1}_{3/2})_n(p_{3/2})_\Lambda]_{0^+}$ and $[(p^{-1}_{1/2})_n(p_{1/2})_\Lambda]_{0^+}$ configurations was almost the same as that of the neutron $p_{1/2}$ and $p_{3/2}$ hole states in ^{15}O, and the splitting of p-state Λ was estimated to be less than 0.3 MeV. In the ${}^{13}\mathrm{C}(K^-,\pi^-){}^{13}_{\Lambda}\mathrm{C}$ experiment at BNL [80], the Λ splitting energy in ${}^{13}_{\Lambda}$C was obtained as 0.36$\pm$0.3 MeV with help of some theoretical consideration on the dominant configurations of the peak. The ${}^9\mathrm{Be}(K^-,\pi^-\gamma){}^9_\Lambda\mathrm{Be}$ experiment at BNL [81] also indicates the small Λ ℓ-s splitting. Only one observed γ-ray peak suggests that the excited doublets $[{}^9\mathrm{Be}(2^+) \otimes (s_{1/2})_\Lambda]_{3/2,5/2}$ are almost degenerate, where the splitting energy has to be less than the experimental resolution of 0.1 MeV. Anyway, the data of Λ ℓ-s splitting energies are yet still far from a quantitative determination.

In Table XIII the values of $S_{LS,ALS}$ and K_Λ for the Nijmegen models are compared to the corresponding ones of nucleons. As stressed in the previous section, the ΛN LS interaction is not so small compared with the NN one, which seemingly is contradictory to the above experimental indications. However, the Λ ℓ-s splitting is likely to be far smaller than the N one due to the reasons mentioned in the previous section. Additionally, the coupling effects with core-excited states also possibly influence the Λ ℓ-s splitting energies. Recently, Dalitz *et al.* [66] analyzed the excited doublet states of ${}^{16}_{\Lambda}$O, whose dominant components are $[(p_{1/2})^{-1}_N(p_{1/2,3/2})_\Lambda]_{0^+,2^+}$. This splitting energy was shown to be understood on the basis of the LS and ALS terms of G-matrix interactions derived from the Nijmegen models, if the coupling to core-excited states with a $(s_{1/2})_\Lambda$ are taken into account. The new experiment at BNL (E929) is now in progress to determine the Λ ℓ-s splitting in ${}^{13}_{\Lambda}$C by detecting the γ-rays from $(p_{3/2})_\Lambda$ and $(p_{1/2})_\Lambda$ states. In order to extract information on the underlying ΛN LS interaction from the coming data, it will be necessary to perform an elaborate structure calculation in which core-excited states are fully taken into account [78].

The spin-orbit interaction is also very interesting from the point of view of the quark model. Namely, the P-wave baryons are hard to describe by the theory if one keeps the full Fermi-Breit spin-orbit interaction from gluon exchange [82]. For the literature since 1980, see Valcarce *et al.* [83]. Here one finds an indication that meson-exchange between quarks $(\pi, \epsilon, \rho, \omega$, etc.) is a possible solution. Another possibility is that the inclusion of the decay channels will be a way out of this problem [84].

ACKNOWLEDGMENTS

Part of this work was done while the first author stayed at the INS, University of Tokyo. We (Th.A.R. and Y.Y) are grateful to Y. Akaishi, T. Harada, and T. Motoba for many stimulating discussions and generous hospitality. V.G.J. Stoks likes to thank T.-S.H. Lee and T. Kuo for their continued interest and constructive comments. We (Th.A.R. and V.G.J.S.) thank J.J. de Swart and R.G.E. Timmermans for discussions, concerning in particularly the scalar meson properties. We are also grateful to K. Miyagawa for performing the three-body calculations for the hypertriton with the NSC97 models. The work of V.G.J.S. was supported in part by the U.S. Department of Energy, Nuclear Physics Division, under Contract No. W-31-109-ENG-38.

APPENDIX: POTENTIAL IN CONFIGURATION SPACE

(a) Pseudoscalar-meson exchange (pseudovector coupling):

$$V_{PV}(r) = \frac{m}{4\pi}\left[f^P_{13}f^P_{24}\left(\frac{m}{m_\pi}\right)^2\left[\tfrac{1}{3}(\boldsymbol{\sigma}_1\cdot\boldsymbol{\sigma}_2)\phi^1_C + S_{12}\phi^0_T\right]\right]. \tag{A1}$$

(b) Vector-meson exchange:

$$\begin{aligned}V_V(r) = \frac{m}{4\pi}\Bigg[\Bigg\{ & g^V_{13}g^V_{24}\left[\phi^0_C + \frac{m^2}{2M_{13}M_{24}}\phi^1_C - \frac{3}{4M_{13}M_{24}}(\Delta\phi^0_C + \phi^0_C\Delta)\right] \\ & + \left[g^V_{13}f^V_{24}\frac{m^2}{4\mathcal{M}M_{24}} + f^V_{13}g^V_{24}\frac{m^2}{4\mathcal{M}M_{13}}\right]\phi^1_C + f^V_{13}f^V_{24}\frac{m^4}{16\mathcal{M}^2M_{13}M_{24}}\phi^2_C\Bigg\}\end{aligned}$$

$$
\begin{aligned}
&+\frac{m^2}{4M_{13}M_{24}}\left\{\left(g^V_{13}+f^V_{13}\frac{M_{13}}{\mathcal{M}}\right)\left(g^V_{24}+f^V_{24}\frac{M_{24}}{\mathcal{M}}\right)\phi^1_C+f^V_{13}f^V_{24}\frac{m^2}{8\mathcal{M}^2}\phi^2_C\right\}\tfrac{2}{3}(\boldsymbol{\sigma}_1\cdot\boldsymbol{\sigma}_2)\\
&-\frac{m^2}{4M_{13}M_{24}}\left\{\left(g^V_{13}+f^V_{13}\frac{M_{13}}{\mathcal{M}}\right)\left(g^V_{24}+f^V_{24}\frac{M_{24}}{\mathcal{M}}\right)\phi^0_T+f^V_{13}f^V_{24}\frac{m^2}{8\mathcal{M}^2}\phi^1_T\right\}S_{12}\\
&-\frac{m^2}{M_{13}M_{24}}\left\{\left[\tfrac{3}{2}g^V_{13}g^V_{24}+g^V_{13}f^V_{24}\frac{M_{24}}{\mathcal{M}}+f^V_{13}g^V_{24}\frac{M_{13}}{\mathcal{M}}\right]\phi^0_{SO}+\tfrac{3}{8}f^V_{13}f^V_{24}\frac{m^2}{\mathcal{M}^2}\phi^1_{SO}\right\}\mathbf{L}\cdot\mathbf{S}\\
&+\frac{m^4}{16M^2_{13}M^2_{24}}\left\{g^V_{13}g^V_{24}+4(g^V_{13}f^V_{24}+f^V_{13}g^V_{24})\frac{\sqrt{M_{13}M_{24}}}{\mathcal{M}}+8f^V_{13}f^V_{24}\frac{M_{13}M_{24}}{\mathcal{M}^2}\right\}\frac{3}{(mr)^2}\phi^0_TQ_{12}\\
&-\frac{m^2}{M_{13}M_{24}}\left\{\left[g^V_{13}g^V_{24}\phi^0_{SO}-f^V_{13}f^V_{24}\frac{m^2}{4\mathcal{M}^2}\phi^1_{SO}\right]\frac{(M^2_{24}-M^2_{13})}{4M_{13}M_{24}}\right.\\
&\qquad\left.-(g^V_{13}f^V_{24}-f^V_{13}g^V_{24})\frac{\sqrt{M_{13}M_{24}}}{\mathcal{M}}\phi^0_{SO}\right\}\tfrac{1}{2}(\boldsymbol{\sigma}_1-\boldsymbol{\sigma}_2)\cdot\mathbf{L}\Bigg]. \qquad\text{(A2)}
\end{aligned}
$$

(c) Scalar-meson exchange:

$$
\begin{aligned}
V_S(r)=-\frac{m}{4\pi}g^S_{13}g^S_{24}\Bigg\{&\left[\phi^0_C-\frac{m^2}{4M_{13}M_{24}}\phi^1_C\right]+\frac{m^2}{2M_{13}M_{24}}\phi^0_{SO}\mathbf{L}\cdot\mathbf{S}+\frac{m^4}{16M^2_{13}M^2_{24}}\frac{3}{(mr)^2}\phi^0_TQ_{12}\\
&+\frac{m^2}{M_{13}M_{24}}\frac{(M^2_{24}-M^2_{13})}{4M_{13}M_{24}}\phi^0_{SO}\tfrac{1}{2}(\boldsymbol{\sigma}_1-\boldsymbol{\sigma}_2)\cdot\mathbf{L}+\frac{1}{4M_{13}M_{24}}(\Delta\phi^0_C+\phi^0_C\Delta)\Bigg\}. \quad\text{(A3)}
\end{aligned}
$$

(d) Diffractive (pomeron-like) exchange:

$$
\begin{aligned}
V_D(r)=\frac{m}{4\pi}g^D_{13}g^D_{24}\frac{4}{\sqrt{\pi}}\frac{m^2}{\mathcal{M}^2}\Bigg[&\Bigg\{1+\frac{m^2}{2M_{13}M_{24}}(3-2m^2r^2)+\frac{m^2}{M_{13}M_{24}}\mathbf{L}\cdot\mathbf{S}+\frac{m^4}{4M^2_{13}M^2_{24}}Q_{12}\\
&+\frac{m^2}{M_{13}M_{24}}\frac{(M^2_{24}-M^2_{13})}{2M_{13}M_{24}}\tfrac{1}{2}(\boldsymbol{\sigma}_1-\boldsymbol{\sigma}_2)\cdot\mathbf{L}\Bigg\}e^{-m^2r^2}\\
&+\frac{1}{4M_{13}M_{24}}(\Delta e^{-m^2r^2}+e^{-m^2r^2}\Delta)\Bigg]. \qquad\text{(A4)}
\end{aligned}
$$

The expressions for the configuration-space functions $\phi^n_X(r)$ can be found in Refs. [1,2], while S_{12} and Q_{12} are the standard tensor and quadratic spin-orbit operators:

$$
\begin{aligned}
S_{12}&=3(\boldsymbol{\sigma}_1\cdot\hat{\mathbf{r}})(\boldsymbol{\sigma}_1\cdot\hat{\mathbf{r}})-(\boldsymbol{\sigma}_1\cdot\boldsymbol{\sigma}_2),\\
Q_{12}&=\tfrac{1}{2}\left[(\boldsymbol{\sigma}_1\cdot\mathbf{L})(\boldsymbol{\sigma}_2\cdot\mathbf{L})+(\boldsymbol{\sigma}_2\cdot\mathbf{L})(\boldsymbol{\sigma}_1\cdot\mathbf{L})\right]. \qquad\text{(A5)}
\end{aligned}
$$

The terms proportional to $(\Delta\phi+\phi\Delta)$ are known as the nonlocal contributions, and represent the explicit momentum-dependent terms (i.e., terms proportional to $\mathbf{q}^2$, the square of the sum of the initial and final momenta) in the momentum-space potential.

In addition to the vector-exchange potential given in Eq. (A2), there is a non-negligible contribution due to the second part of the vector-meson propagator, $k_\mu k_\nu/m^2$. Its structure is similar to the scalar-exchange potential given in Eq. (A3), and so we have

$$
V_V(r)\rightarrow V_V(r)-\frac{(M_3-M_1)(M_4-M_2)}{m^2}V_S(r), \qquad\text{(A6)}
$$

where in $V_S(r)$, obviously, now the vector-meson coupling constants have to be used. Also, it is clear that this part only contributes when both $M_3\neq M_1$ and $M_4\neq M_2$.

REFERENCES

[1] M.M. Nagels, T.A. Rijken, and J.J. de Swart, Phys. Rev. D **17**, 768 (1978).

[2] P.M.M. Maessen, Th.A. Rijken, and J.J. de Swart, Phys. Rev. C **40**, 2226 (1989).

[3] T.A. Rijken, Ann. Phys. (N.Y.) **164**, 1, 23 (1985).

[4] Y. Yamamoto and H. Bandō, Prog. Theor. Phys. **83**, 254 (1990).

[5] T. Motoba and Y. Yamamoto, Nucl. Phys. **A585**, 29c (1995).

[6] T. Hasegawa *et al.*, Phys. Rev. Lett. **74**, 224 (1995).

[7] L. Micu, Nucl. Phys. **B10**, 521 (1969); R. Carlitz and M. Kislinger, Phys. Rev. D **2**, 336 (1970).

[8] O. Dumbrajs, R. Koch, H. Pilkuhn, G.C. Oades, H. Behrens, J.J. de Swart, and P. Kroll, Nucl. Phys. **B216**, 277 (1983).

[9] J.J. Sakurai, Ann. Phys. (N.Y.) **11**, 1 (1960).

[10] B. Sakita and K.C. Wali, Phys. Rev. **139**, B1355 (1965).

[11] R.H. Dalitz and F. von Hippel, Phys. Lett. **10**, 153 (1964).

[12] J.J. de Swart, Rev. Mod. Phys. **35**, 916 (1963); *ibid.* **37**, 326(E) (1965).

[13] Th.A. Rijken and P.M.M. Maessen, unpublished.

[14] Th.A. Rijken and V.G.J. Stoks, Phys. Rev. C **46**, 73, 102 (1992).

[15] Th.A. Rijken and V.G.J. Stoks, Phys. Rev. C **54**, 2851, 2869 (1996).

[16] R.H. Thompson, Phys. Rev. D **1**, 110 (1970).

[17] Th.A. Rijken, R.A.M. Klomp, and J.J. de Swart, in *Essays in Celebration of the Life of Robert Eugene Marshak*, edited by E.C.G. Sudarshan, (World Scientific, Singapore, 1995).

[18] H.P. Noyes, Phys. Rev. Lett. **15**, 538 (1965).

[19] K.L. Kowalski, Phys. Rev. Lett. **15**, 798 (1965).

[20] C.M. Vincent and S.C. Phatak, Phys. Rev. C **10**, 391 (1974).

[21] J.R.M. Bergervoet, Ph.D. thesis, University of Nijmegen, 1987 (unpublished).

[22] M.M. Nagels, T.A. Rijken, and J.J. de Swart, Ann. Phys. (N.Y.) **79**, 338 (1973).

[23] J.J. de Swart, Th.A. Rijken, P.M. Maessen, and R. Timmermans, Nuovo Cim. **102A**, 203 (1989).

[24] M.M. Nagels, T.A. Rijken, and J.J. de Swart, Phys. Rev. D **12**, 744 (1975).

[25] M.M. Nagels, T.A. Rijken, and J.J. de Swart, Phys. Rev. D **15**, 2547 (1977).

[26] M.M. Nagels, T.A. Rijken, and J.J. de Swart, Phys. Rev. D **20**, 1633 (1979).

[27] J.J. de Swart, P.M.M. Maessen, and Th.A. Rijken, in *Properties and Interactions of Hyperons*, Proceedings of the U.S.-Japan Seminar, Maui 1993, eds. B.F. Gibson, P.D. Barnes, and K. Nakai (World Scientific, 1994), p. 37.

[28] N. Hoshizaki, I. Lin, and S. Machida, Prog. Theor. Phys. **24**, 480 (1960); N. Hoshizaki, S. Otsuki, W. Watari, and M. Yonezawa, Prog. Theor. Phys. **27**, 1199 (1962).

[29] J. Schwinger, Phys. Rev. D **3**, 1967 (1971).

[30] J. Binstock and R.A. Bryan, Phys. Rev. D **4**, 1341 (1971); R.A. Bryan and A. Gersten, Phys. Rev. D **6**, 341 (1972).

[31] M. Svec, A. de Lesquen, and L. van Rossum, Phys. Rev. D **46**, 949 (1992); M. Svec, Phys. Rev. D **53**, 2343 (1996).

[32] M. Svec, A. de Lesquen, and L. van Rossum, Phys. Rev. D **45**, 1518 (1992).

[33] Particle Data Group (PDG), R.M. Barnett *et al.*, Phys. Rev. D **54**, 1 (1996).

[34] F.J. Gilman and H. Harari, Phys. Rev. **165**, 1803 (1968).
[35] S. Weinberg, Phys. Phys. **166**, 1568 (1968); *ibid.* **177**, 2604 (1969).
[36] S. Weinberg, Phys. Rev. Lett. **65**, 1177 (1990).
[37] N.A. Törnqvist, Z. Phys. C **68**, 647 (1995); N.A. Törnqvist and M. Roos, Phys. Rev. Lett. **76**, 1575 (1996).
[38] R.L. Jaffe, Phys. Rev. D **15**, 267, 281 (1977).
[39] R.H. Dalitz, D.H. Davis, P.H. Fowler, A. Montwill, J. Pniewski, and J.A. Zakrewski, Proc. Roy. Soc. (London) **A426**, 1 (1989).
[40] F.E. Low, Phys. Rev. D **12**, 163 (1975); S. Nussinov, Phys. Rev. Lett. **34**, 1286 (1975).
[41] J. Pumplin and E. Lehman, Z. Phys. C **9**, 25 (1981); J.F. Gunion and D.E. Soper, Phys. Rev. D **9**, 2617 (1977).
[42] A.M. Smith *et al.*, Phys. Lett. B **163**, 267 (1985).
[43] T. Henkes *et al.*, Phys. Lett. B **283**, 155 (1992).
[44] P.V. Landshoff and O. Nachtmann, Z. Phys. C **35**, 405 (1987).
[45] S. Weinberg, Phys. Rev. Lett. **18**, 507 (1967).
[46] A. Le Yaouanc, L. Oliver, O. Péne, and J.-C. Raynal, Phys. Rev. D **8**, 2223 (1973); M. Chaichain and R. Kögerler, Ann. Phys. (N.Y.) **124**, 61 (1980).
[47] K.J. Barnes, P. Carruthers, and F. von Hippel, Phys. Rev. Lett. **14**, 82 (1965); H.J. Lipkin and S. Meshkov, Phys. Rev. Lett. **14**, 670 (1965) and Phys. Rev. **143**, 1269 (1966).
[48] G. Alexander, U. Karshon, A. Shapira, G. Yekutieli, R. Engelmann, H. Filthuth, and W. Lughofer, Phys. Rev. **173**, 1452 (1968).
[49] B. Sechi-Zorn, B. Kehoe, J. Twitty, and R.A. Burnstein, Phys. Rev. **175**, 1735 (1968).
[50] F. Eisele, H. Filthuth, W. Fölisch, V. Hepp, E. Leitner, and G. Zech, Phys. Lett. **37B**, 204 (1971).
[51] R. Engelmann, H. Filthuth, V. Hepp, and E. Kluge, Phys. Lett. **21**, 587 (1966).
[52] V. Hepp and M. Schleich, Z. Phys. **214**, 71 (1968).
[53] J.A. Kadyk, G. Alexander, J.H. Chan, P. Gaposchkin, and G.H. Trilling, Nucl. Phys. **B27**, 13 (1971).
[54] J.M. Hauptman, J.A. Kadyk, and G.H. Trilling, Nucl. Phys. **B125**, 29 (1977).
[55] B. Holzenkamp, K. Holinde, and J. Speth, Nucl. Phys. **A500**, 485 (1989).
[56] A. Reuber, K. Holinde, and J. Speth, Nucl. Phys. **A570**, 543 (1994).
[57] Y. Yamamoto and H. Bandō, Prog. Theor. Phys. **73**, 905 (1985); Prog. Theor. Phys. Suppl. **81**, 42 (1985).
[58] Y. Yamamoto, T. Motoba, H. Himeno, K. Ikeda, and S. Nagata, Prog. Theor. Phys. Suppl. **117**, 361 (1994).
[59] D.J. Millener, A. Gal, and C.B. Dover, Phys. Rev. C **38**, 2700 (1988).
[60] P.H. Pile *et al.*, Phys. Rev. Lett. **66**, 2585 (1991).
[61] T. Hasegawa *et al.*, Phys. Rev. C **53**, 1210 (1996).
[62] H.-J. Schulze, A. Lejeune, J. Cugnon, M. Baldo, and U. Lombardo, Phys. Lett. B **355**, 21 (1995) and Phys. Rev. C **57**, 704 (1998).
[63] R.R. Scheerbaum, Nucl. Phys. **A257**, 77 (1976).
[64] D.W.L. Sprung, Nucl. Phys. **A182**, 97 (1972).
[65] K. Andō and H. Bandō, Prog. Theor. Phys. **66**, 227 (1981).
[66] R.H. Dalitz, D.H. Davis, T. Motoba, and D.N. Tovee, Nucl. Phys. **A625** 71 (1997).

[67] T. Nagae *et al.*, Phys. Rev. Lett. **80**, 1605 (1998).
[68] T. Harada, S. Shinmura, Y. Akaishi, and H. Tanaka, Nucl. Phys. **A507**, 715 (1990).
[69] Y.C. Tang and B.C. Herndon, Phys. Rev. **138**, B637 (1965).
[70] A.R. Bodmer and S. Ali, Phys. Rev. **138**, B644 (1965).
[71] M. Bedjidian *et al.*, Phys. Lett. **62B**, 467 (1976); *ibid.* **83B**, 252 (1979).
[72] K. Miyagawa and W. Glöckle, Phys. Rev. C **48**, 2576 (1993).
[73] K. Miyagawa, H. Kamada, W. Glöckle, and V. Stoks, Phys. Rev. C **51**, 2905 (1995).
[74] K. Miyagawa, private communication.
[75] J.A. Carlson, in *Proceedings of the LAMPF Workshop on* (π, K) *Physics*, 1991, AIP Conference Proceedings, Vol. 224, p. 198; J. Carlson and B. Gibson, Particles and Fields **43**, 198 (1990).
[76] T. Motoba, private communication.
[77] H. Tamura, in *Proceedings of the International Conference on Hypernuclear and Strange Particle Physics*, Oct. 13-18, 1997, Brookhaven National Laboratory, U.S.A.; Nucl. Phys. A (1998), to be published.
[78] E. Hiyama *et al.*, in *Proceedings of the International Conference on Hypernuclear and Strange Particle Physics*, Oct. 13-18, 1997, Brookhaven National Laboratory, U.S.A.; Nucl. Phys. A (1998), to be published.
[79] W. Brückner *et al.*, Phys. Lett. **79B**, 157 (1978).
[80] M. May *et al.*, Phys. Rev. Lett. **47**, 1106 (1981).
[81] M. May *et al.*, Phys. Rev. Lett. **51**, 2085 (1983).
[82] N. Isgur and G. Karl, Phys. Rev. D **18**, 4187 (1978); *ibid.* **19**, 2653 (1979).
[83] A. Valcarce, A. Buchmann, F. Fernández, and A. Faessler, Phys. Rev. C **51**, 1480 (1995).
[84] Y. Fujiwara, Prog. Theor. Phys. **90**, 105 (1993).

FIGURES

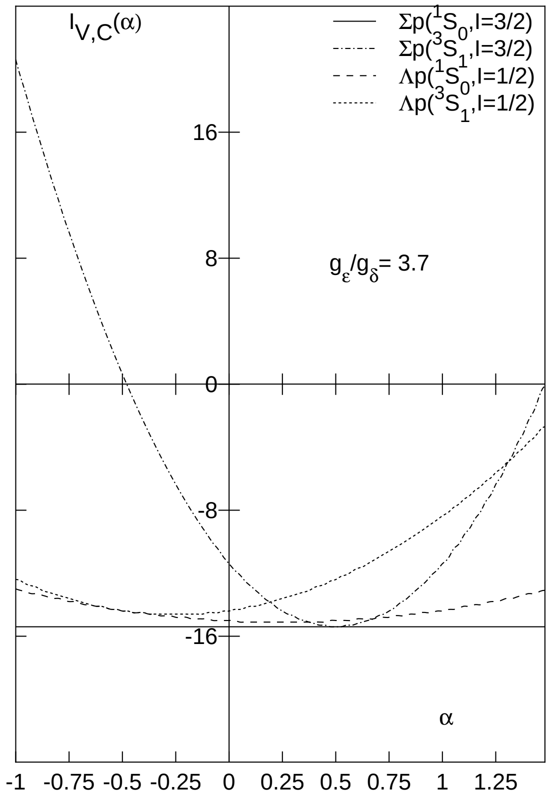

FIG. 1. Volume integral for the scalar-exchange central YN potentials in arbitrary units.

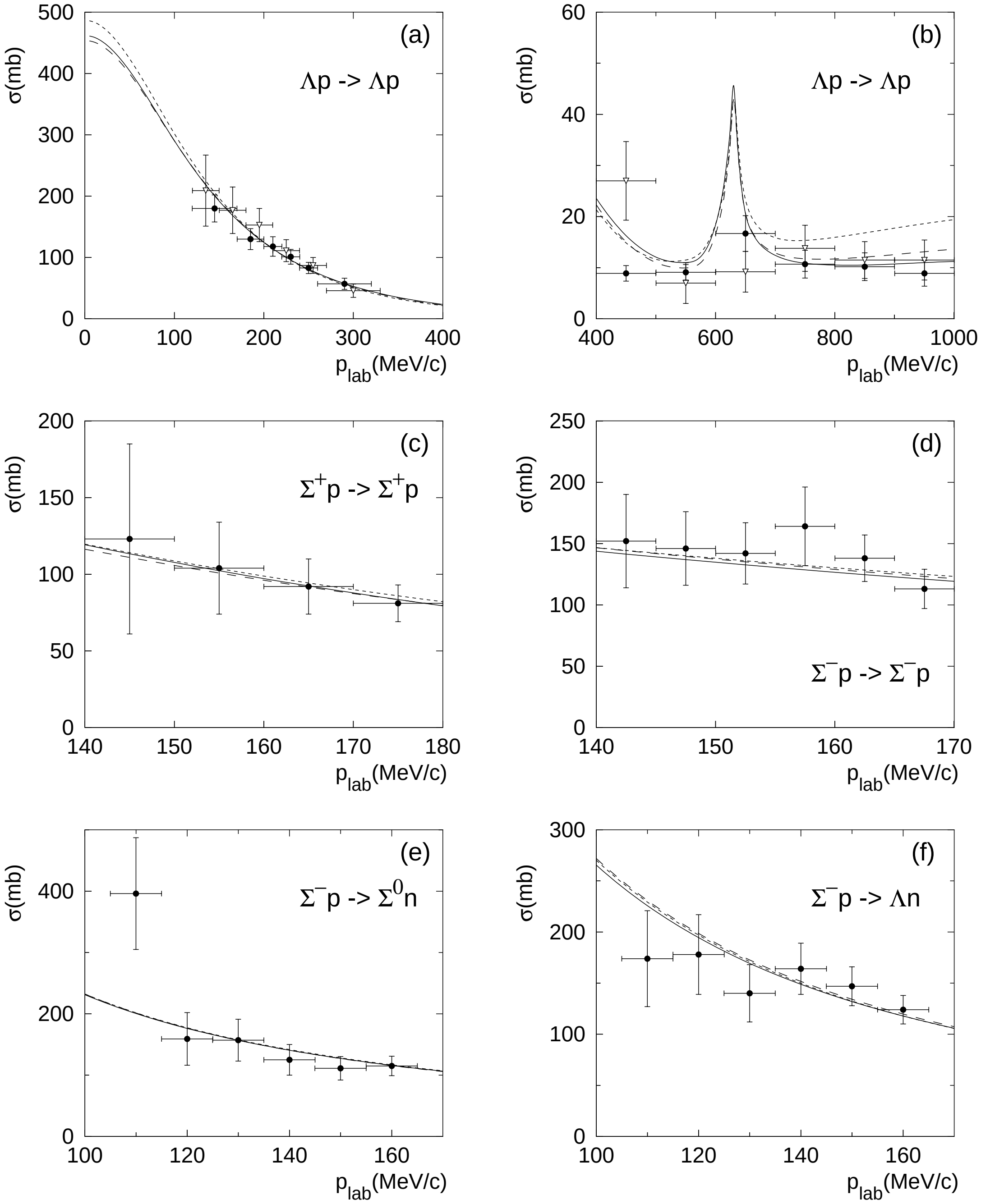

FIG. 2. Calculated total cross sections compared with experimental data. Solid curve: NSC97a; dashed curve: NSC97c; dotted curve: NSC97f. Experimental data in (a) from Ref. [48] (closed circles) and Ref. [49] (open triangles); in (b) from Ref. [53] (closed circles) and Ref. [54] (open triangles); in (c) and (d) from Ref. [50]; and in (e) and (f) from Ref. [51].

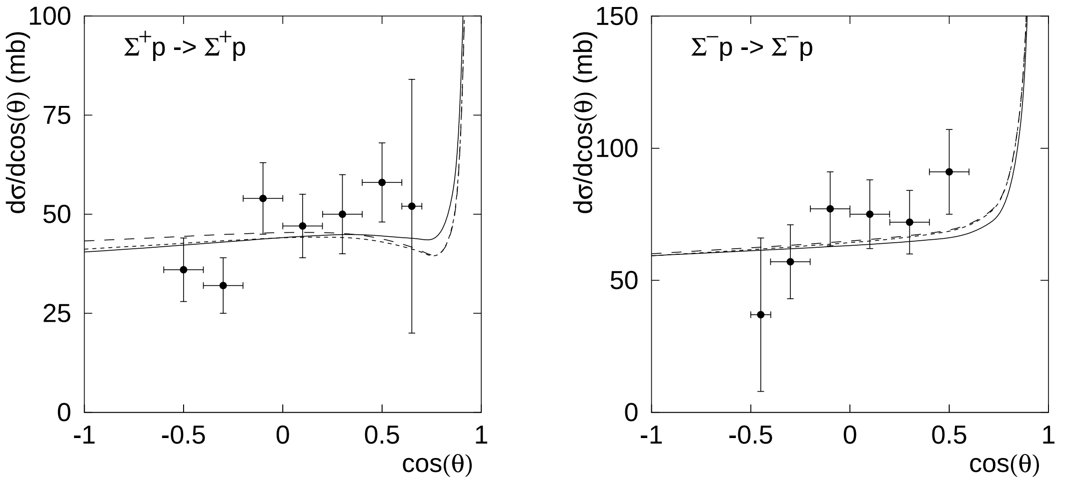

FIG. 3. Predictions for differential cross sections for models NSC97a (solid line), NSC97c (dotted line), and NSC97f (dash-dotted line). Experimental data from Ref. [50].

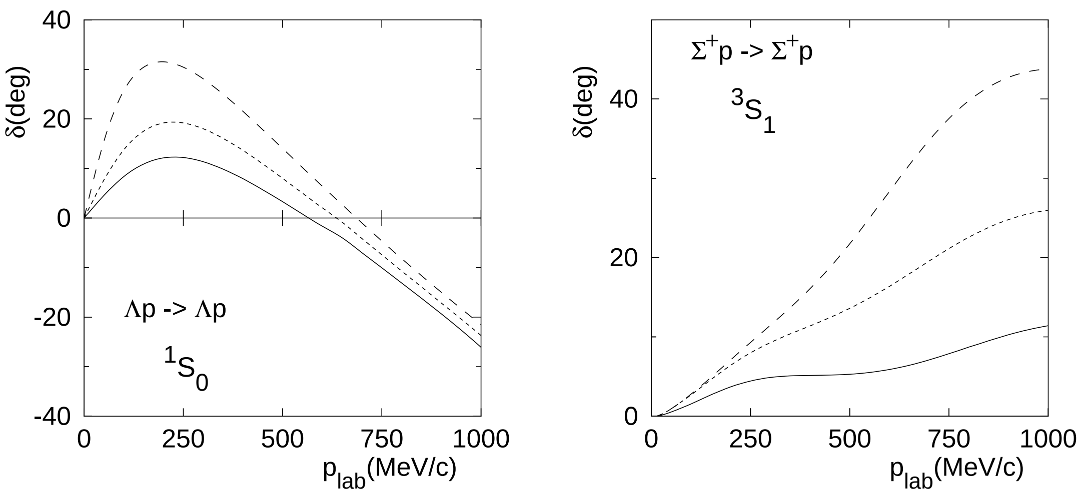

FIG. 4. $\Lambda p\ ^1S_0$ phase shifts for models NSC97a (solid line), NSC97c (dotted line), and NSC97f (dash-dotted line).

TABLES

TABLE I. Isospin factors for the various meson exchanges in the two isospin channels. P is the exchange operator (see text).

Matrix element	$I=\frac{1}{2}$	$I=\frac{3}{2}$
$(\Lambda N\vert\eta\vert\Lambda N)$	1	0
$(\Lambda N\vert\eta'\vert\Lambda N)$	1	0
$(\Lambda N\vert\pi\vert\Lambda N)$	-0.0283	0
$(\Lambda N\vert K\vert N\Lambda)$	P	0
$(\Sigma N\vert\eta\vert\Sigma N)$	1	1
$(\Sigma N\vert\eta'\vert\Sigma N)$	1	1
$(\Sigma N\vert\pi\vert\Sigma N)$	-2	1
$(\Sigma N\vert K\vert N\Sigma)$	$-P$	$2P$
$(\Lambda N\vert\pi\vert\Sigma N)$	$-\sqrt{3}$	0
$(\Lambda N\vert K\vert N\Sigma)$	$-P\sqrt{3}$	0
$(\Sigma N\vert\pi\vert\Lambda N)$	$-\sqrt{3}$	0
$(\Sigma N\vert K\vert N\Lambda)$	$-P\sqrt{3}$	0

TABLE II. Coupling constants, $F/(F+D)$ ratios α, mixing angles, and cut-off parameters in MeV/c^2, common to all six models. Singlet refers to the *physical* meson, i.e., η', ω, ε, and pomeron. Subscripts 8, 1, and K on the cut-off parameter Λ refer to isovector, isoscalar, and strange (isodoublet) mesons within the meson nonet, respectively. A dash means this parameter differs from one model to the next.

Mesons		Singlet	Octet	α	Angles	Λ_8	Λ_1	Λ_K
Pseudoscalar	$f/\sqrt{4\pi}$	0.14410	0.27286	0.355	–23.0°	1254.63	872.09	1281.64
Vector	$g/\sqrt{4\pi}$	2.92133	0.83689	1.000	37.5°	895.07	949.33	1184.52
	$f/\sqrt{4\pi}$	1.18335	3.53174	–				
Scalar	$g/\sqrt{4\pi}$	4.59789	1.39511	–	–	548.72	988.99	935.75
Diffractive	$g/\sqrt{4\pi}$	2.86407	0.0	0.250	0.0°			

TABLE III. Fitted scalar-meson mixing angle, θ_S, and flavor-symmetry breaking parameters, $\lambda_{\rm fsb}$, for models NSC97a–f. Note that the scalar $F/(F+D)$ ratio α_S was not fitted, but is determined by Eq. (4.7).

Model	α_V^m	θ_S	α_S	$\lambda_{\rm fsb}^P$	$\lambda_{\rm fsb}^V$	$\lambda_{\rm fsb}^S$
(a)	0.4447	37.07°	1.086	0.957	0.828	0.918
(b)	0.4247	37.32°	1.091	1.003	0.895	0.946
(c)	0.4047	37.57°	1.096	1.022	0.985	0.990
(d)	0.3847	38.31°	1.111	1.084	1.090	1.037
(e)	0.3747	38.88°	1.123	1.137	1.145	1.061
(f)	0.3647	39.65°	1.138	1.242	1.188	1.070

TABLE IV. χ^2 results on the 35 YN experimental total cross sections for the six different models, labeled according to the α_V^m input (see Table III. The last column gives the predictions for the capture ratio at rest.

Model	$\Lambda p \to \Lambda p$ Ref. [48]	$\Lambda p \to \Lambda p$ Ref. [49]	$\Sigma^+ p \to \Sigma^+ p$ Ref. [50]	$\Sigma^- p \to \Sigma^- p$ Ref. [50]	$\Sigma^- p \to \Sigma^0 n$ Ref. [51]	$\Sigma^- p \to \Lambda n$ Ref. [51]	$r_R^{\rm th}$ Ref. [52]
(a)	1.63	2.12	0.07	2.28	5.90	3.68	0.469
(b)	1.59	2.22	0.06	2.32	5.82	3.77	0.466
(c)	1.78	2.00	0.08	1.98	5.86	3.90	0.469
(d)	1.98	1.93	0.10	1.89	5.84	4.01	0.468
(e)	2.29	1.89	0.10	1.89	5.88	4.00	0.468
(f)	2.52	2.04	0.20	1.95	6.01	3.94	0.467

TABLE V. Singlet $^1S_0$ and triplet $^3S_1$ scattering lengths for models NSC97a–f in the different channels.

	$\Sigma^+ p$		Λp		Λn		$\Sigma^- n$	
Model	$^1S_0$	$^3S_1$	$^1S_0$	$^3S_1$	$^1S_0$	$^3S_1$	$^1S_0$	$^3S_1$
(a)	–4.35	–0.14	–0.71	–2.18	–0.76	–2.14	–6.13	–0.15
(b)	–4.32	–0.17	–0.90	–2.13	–0.97	–2.08	–6.06	–0.18
(c)	–4.28	–0.25	–1.20	–2.08	–1.28	–2.06	–5.98	–0.28
(d)	–4.23	–0.29	–1.71	–1.95	–1.82	–1.93	–5.89	–0.33
(e)	–4.23	–0.28	–2.10	–1.86	–2.24	–1.82	–5.90	–0.32
(f)	–4.35	–0.25	–2.51	–1.75	–2.68	–1.66	–6.16	–0.29

TABLE VI. $\Sigma^+ p$ nuclear bar phase shifts in degrees for NSC97f.

p_{Σ^+} (MeV/c)	200	400	600	800	1000
$T_{\rm lab}$ (MeV)	16.7	65.5	142.8	244.0	364.5
$^1S_0$	42.01	28.67	11.86	–3.82	–17.81
$^3P_0$	4.92	9.79	4.51	–5.48	–16.48
$^1P_1$	2.55	9.36	13.70	12.40	7.39
$^3P_1$	–3.03	–9.72	–17.07	–24.94	–32.92
$^3S_1$	7.11	16.10	28.36	39.79	43.80
ε_1	–1.90	–2.82	0.08	3.16	4.23
$^3D_1$	0.26	1.20	1.31	–1.26	–6.60
$^1D_2$	0.29	1.88	5.01	8.90	11.70
$^3D_2$	–0.43	–2.24	–4.23	–6.51	–9.49
$^3P_2$	0.79	4.43	8.01	9.60	9.83
ε_2	–0.36	–1.84	–3.00	–3.20	–2.60
$^3F_2$	0.03	0.38	0.83	0.76	–0.41

TABLE VII. Λp nuclear bar phase shifts in degrees for NSC97f.

p_Λ (MeV/c)	100	200	300	400	500	600	633.4
$T_{\rm lab}$ (MeV)	4.5	17.8	39.6	69.5	106.9	151.1	167.3
$^1S_0$	25.68	31.52	28.08	21.52	14.03	6.42	3.92
$^3P_0$	0.02	0.05	–0.39	–2.01	–5.10	–9.42	–11.00
$^1P_1$	–0.08	–0.59	–1.82	–3.88	–6.71	–10.08	–11.24
$^3P_1$	–0.09	–0.74	–2.38	–5.04	–8.47	–12.12	–13.06
$^3S_1$	19.26	25.92	24.76	20.57	15.62	11.55	7.68
ε_1	0.16	0.81	1.80	3.03	4.77	10.18	19.81
$^3D_1$	0.00	0.05	0.36	1.49	5.15	23.26	76.52
$^1D_2$	0.00	0.05	0.30	0.96	2.08	3.54	4.07
$^3D_2$	0.00	0.08	0.44	1.27	2.61	4.32	4.95
$^3P_2$	0.05	0.31	0.59	0.52	–0.16	–1.45	–1.99
ε_2	–0.00	–0.01	–0.10	–0.31	–0.62	–0.99	–1.11
$^3F_2$	0.00	0.00	0.01	0.06	0.19	0.47	0.70

TABLE VIII. $\Lambda p \rightarrow \Lambda p, \Sigma^+ n, \Sigma^0 p$ total cross sections in mb above the ΣN thresholds for NSC97f.

p_Λ (MeV/c)	$T_{\rm lab}$ (MeV)	$\Lambda p \rightarrow \Lambda p$	$\Lambda p \rightarrow \Sigma^+ n$	$\Lambda p \rightarrow \Sigma^0 p$
650	175.5	23.30	8.11	2.90
700	201.4	15.87	7.80	3.68
750	228.7	15.34	7.39	3.59
800	257.2	15.94	6.93	3.41
850	286.9	16.82	6.50	3.22
900	317.8	17.73	6.12	3.04
950	349.7	18.60	5.79	2.88
1000	382.6	19.40	5.50	2.74

TABLE IX. $\Sigma^- p \to \Sigma^- p, \Sigma^0 n, \Lambda n$ total nuclear cross sections in mb above the ΣN thresholds for NSC97f.

p_{Σ^-} (MeV/c)	$T_{\rm lab}$ (MeV)	$\Sigma^- p \to \Sigma^- p$	$\Sigma^- p \to \Sigma^0 n$	$\Sigma^- p \to \Lambda n$
50	1.0	427.8	672.8	862.3
100	4.2	211.8	232.3	270.2
150	9.4	143.2	128.1	132.5
200	16.6	107.8	85.3	78.4
250	25.8	86.0	62.7	51.9
300	37.0	71.4	48.8	37.0
350	50.1	60.9	39.4	28.0
400	65.0	53.2	32.6	22.1
450	81.8	47.3	27.5	18.1
500	100.2	42.7	23.5	15.3

TABLE X. Partial-wave contributions to the Λ potential energy $U_\Lambda(k_\Lambda = 0)$ at $k_F = 1.35$ fm^{-1} in the cases of NSC97 models. G-matrix calculations are performed with the QTQ prescription for intermediate spectra. All entries are in MeV.

Model	$^1S_0$	$^3S_1$	$^1P_1$	$^3P_0$	$^3P_1$	$^3P_2$	Sum
(a)	–3.8	–30.7	1.5	–0.2	1.6	–2.2	–33.9
(b)	–5.5	–30.0	1.6	–0.1	1.9	–2.1	–34.1
(c)	–7.8	–29.7	1.7	0.2	2.2	–1.9	–35.3
(d)	–11.0	–27.7	1.9	0.4	2.7	–1.5	–35.1
(e)	–12.8	–26.0	2.1	0.5	3.2	–1.2	–34.3
(f)	–14.4	–22.9	2.4	0.5	4.0	–0.7	–31.1

TABLE XI. Contributions to U_Λ at $k_F = 1.35$ fm^{-1} from spin-independent, spin-spin, LS, and tensor parts of the G-matrix interactions. See the text for the definitions of U_0, $U_{\sigma\sigma}$, U_{LS}, and U_T. All entries are in MeV.

	S-states		P-states			
Model	$U_0(S)$	$U_{\sigma\sigma}(S)$	$U_0(P)$	$U_{\sigma\sigma}(P)$	$U_{LS}(P)$	$U_T(P)$
(a)	–8.62	–1.61	0.30	–0.39	–0.28	0.17
(b)	–8.88	–1.13	0.38	–0.41	–0.32	0.17
(c)	–9.37	–0.52	0.46	–0.40	–0.37	0.15
(d)	–9.67	0.43	0.61	–0.42	–0.43	0.15
(e)	–9.70	1.04	0.72	–0.44	–0.46	0.17
(f)	–9.33	1.68	0.92	–0.50	–0.47	0.22
NSC89	–6.00	3.10	0.27	–0.43	–0.53	0.14
NHC-F	–7.67	0.77	0.13	–0.39	–0.49	0.14
NHC-D	–8.13	–0.24	–1.08	0.46	–0.44	0.09

TABLE XII. Comparison between the QTQ and CIES treatments for the intermediate spectrum. See the text for the definitions of U_0, $U_{\sigma\sigma}$, U_{LS}, and U_T. All entries are in MeV.

	$k_F = 1.35$ fm^{-1}		$k_F = 1.0$ fm^{-1}	
	QTQ	CIES	QTQ	CIES
U_Λ	–31.1	–34.3	–19.9	–21.9
$U_0(S)$	–9.33	–9.96	–5.25	–5.73
$U_{\sigma\sigma}(S)$	1.68	1.58	0.66	0.66
$U_0(P)$	0.92	0.83	0.18	0.16
$U_{\sigma\sigma}(P)$	–0.50	–0.47	–0.11	–0.10
$U_{LS}(P)$	–0.47	–0.44	–0.10	–0.09
$U_T(P)$	0.22	0.14	0.06	0.05

TABLE XIII. Strengths of Λ spin-orbit splittings for various Nijmegen models. See the text for the definitions of K_B and $S_{LS,ALS}$. The corresponding ones for the NN interaction (G0) are also shown.

Model	S_{LS}	S_{ALS}	K_B
(a)	–14.2	6.2	8.
(b)	–16.2	6.4	10.
(c)	–18.9	6.7	13.
(d)	–21.7	7.1	15.
(e)	–23.1	7.2	17.
(f)	–23.9	7.0	18.
NSC89	–28.0	7.9	21.
NHC-F	–22.8	5.0	19.
NHC-D	–22.0	7.3	15.
G0(NN)	–36.4		57.

TABLE XIV. Contributions to U_Σ at $k_F = 1.0$ fm^{-1} in the cases of NSC97e, NSC97f, NSC89, NHC-F, and NHC-D. Conversion widths Γ_Σ are also shown. All entries are in MeV.

	Isospin $T = 1/2$			Isospin $T = 3/2$				
Model	$^1S_0$	$^3S_1$	P	$^1S_0$	$^3S_1$	P	Sum	Γ_Σ
NSC97e	5.2	–7.5	0.0	–6.1	–2.5	–0.9	–11.8	14.6
NSC97f	5.2	–7.6	0.0	–6.1	–2.2	–0.9	–11.5	15.5
NSC89	3.0	–4.2	–0.3	–5.8	3.7	0.1	–3.6	25.0
NHC-F	4.2	–10.9	–1.5	–5.3	18.6	–1.7	3.5	16.3
NHC-D	2.1	–9.6	–2.2	–5.4	9.4	–3.0	–8.7	8.7